

ACCEPTED MANUSCRIPT



A  $K^+$ -selective CNG channel orchestrates  $Ca^{2+}$  signalling in zebrafish sperm

Sylvia Fechner, Luis Alvarez, Wolfgang Bönigk, Astrid Müller, Thomas Berger, Rene Pascal, Christian Trötschel, Ansgar Poetsch, Gabriel Stöting, Kellee R Siegfried, Elisabeth Kremmer, Reinhard Seifert, U Benjamin Kaupp

DOI: <http://dx.doi.org/10.7554/eLife.07624>

Cite as: eLife 2015;10.7554/eLife.07624

Received: 20 March 2015

Accepted: 9 December 2015

Published: 9 December 2015

This PDF is the version of the article that was accepted for publication after peer review. Fully formatted HTML, PDF, and XML versions will be made available after technical processing, editing, and proofing.

Stay current on the latest in life science and biomedical research from eLife.  
[Sign up for alerts](http://elife.elifesciences.org) at [elife.elifesciences.org](http://elife.elifesciences.org)

1 **A K<sup>+</sup>-selective CNG channel orchestrates Ca<sup>2+</sup> signalling in zebrafish sperm**

2 Condensed title: Signalling in zebrafish sperm

3  
4 Fechner, S.<sup>1</sup>, Alvarez, L.<sup>1</sup>, Bönigk, W.<sup>1</sup>, Müller, A.<sup>1</sup>, Berger, T.<sup>1</sup>, Pascal, R.<sup>1</sup>, Trötschel, C.<sup>2</sup>,  
5 Poetsch, A.<sup>2</sup>, Stölting, G.<sup>5</sup>, Siegfried, K.R.<sup>3</sup>, Kremmer, E.<sup>4</sup>, Seifert, R.<sup>1</sup>, and Kaupp, U.B.<sup>1</sup>

6  
7  
8 <sup>1</sup>Center of Advanced European Studies and Research (caesar), Abteilung Molekulare Neurosensorik,  
9 Ludwig-Erhard-Allee 2, 53175 Bonn, Germany; <sup>2</sup>Ruhr-Universität Bochum, Lehrstuhl Biochemie der  
10 Pflanzen, Universitätsstr. 150, 44801 Bochum, Germany; <sup>3</sup>University of Massachusetts Boston, Biology  
11 Department, 100 Morrissey Blvd., Boston, MA 02125-3393; <sup>4</sup>Helmholtz-Zentrum München, Institut für  
12 Molekulare Immunologie, Marchioninstr. 25, 81377 München, Germany. <sup>5</sup>Research Centre Jülich,  
13 Institute of Complex Systems 4 (ICS-4), 52425 Jülich, Germany.

14  
15  
16  
17  
18 Send correspondence to: U. Benjamin Kaupp  
19 Center of Advanced European Studies and Research  
20 Ludwig-Erhard-Allee 2  
21 53175 Bonn, Germany  
22 Tel.: ++49228-9656-100, Fax: ++49228-9656-9100  
23 e-mail: [u.b.kaupp@caesar.de](mailto:u.b.kaupp@caesar.de)

24  
25  
26 Sylvia Fechner  
27 Center of Advanced European Studies and Research  
28 Ludwig-Erhard-Allee 2  
29 53175 Bonn, Germany  
30 Present Address Department of Molecular and Cellular Physiology  
31 Stanford University  
32 Stanford, California 94305, USA  
33 e-mail: [sfechner@stanford.edu](mailto:sfechner@stanford.edu)

34  
35  
36  
37 Keywords: Zebrafish; sperm signalling; fertilization; potassium channel

## 40 **Abstract**

41 Calcium in the flagellum controls sperm navigation. In sperm of marine invertebrates and  
42 mammals,  $\text{Ca}^{2+}$  signalling has been intensely studied, whereas for fish little is known. In sea  
43 urchin sperm, a cyclic nucleotide-gated  $\text{K}^+$  channel (CNGK) mediates a cGMP-induced  
44 hyperpolarization that evokes  $\text{Ca}^{2+}$  influx. Here, we identify in sperm of the freshwater fish  
45 *Danio rerio* a novel CNGK family member featuring non-canonical properties. It is located in  
46 the sperm head rather than the flagellum and is controlled by intracellular pH, but not cyclic  
47 nucleotides. Alkalization hyperpolarizes sperm and produces  $\text{Ca}^{2+}$  entry.  $\text{Ca}^{2+}$  induces  
48 spinning-like swimming, different from swimming of sperm from other species. The  
49 “spinning” mode probably guides sperm into the micropyle, a narrow entrance on the surface  
50 of fish eggs. A picture is emerging of sperm channel orthologues that employ different  
51 activation mechanisms and serve different functions. The channel inventories probably reflect  
52 adaptations to species-specific challenges during fertilization.

53

## 54 **Introduction**

55 Fertilization is a complex task that, for different species, happens in entirely different spatial  
56 compartments or ionic milieus. In aquatic habitats, gametes are released into the water where  
57 sperm acquire motility and navigate to the egg. By contrast, mammalian fertilization happens  
58 in confined compartments of the female oviduct. From invertebrates to mammals, sperm use  
59 various sensing mechanisms, including chemotaxis, rheotaxis, and thermotaxis, to gather  
60 physical or chemical cues to spot the egg. These sensory cues activate various cellular  
61 signalling pathways that ultimately control the intracellular  $\text{Ca}^{2+}$  concentration ( $[\text{Ca}^{2+}]_i$ ) and,  
62 thereby, the flagellar beat and swimming behaviours (Alvarez et al., 2012; Darszon et al.,  
63 2008; Eisenbach and Giojalas, 2006; Florman et al., 2008; Guerrero et al., 2010; Ho and

64 Suarez, 2001; Kaupp et al., 2008; Publicover et al., 2008). In species as phylogenetically  
65 distant as sea urchin and mammals, these pathways target a sperm-specific, voltage-dependent  
66  $\text{Ca}^{2+}$  channel, called CatSper. Signalling events open CatSper by shifting its voltage-  
67 dependence to permissive, more negative  $V_m$  values. This shift is achieved by different  
68 means. In sea urchin sperm, opening of a  $\text{K}^+$ -selective cyclic nucleotide-gated channel  
69 (CNGK) causes a transient hyperpolarization (Bönigk et al., 2009; Strünker et al., 2006); the  
70 hyperpolarization activates a sperm-specific  $\text{Na}^+/\text{H}^+$  exchanger (sNHE) (Lee, 1984, 1985; Lee  
71 and Garbers, 1986) resulting in a long-lasting alkalization that shifts the voltage dependence  
72 of CatSper and leads to a  $\text{Ca}^{2+}$  influx (Kaupp et al., 2003; Seifert et al., 2015). By contrast, in  
73 human sperm, the shift is achieved by direct stimulation of CatSper with prostaglandins and  
74 progesterone in the seminal fluid or the oviduct (Brenker et al., 2012; Lishko et al., 2011;  
75 Smith et al., 2013; Strünker et al., 2011).

76 Navigation of fish sperm and the underlying signalling pathways must be arguably different.  
77 First, teleost fish are lacking CatSper channels (Cai and Clapham, 2008), although activation  
78 of sperm motility requires  $\text{Ca}^{2+}$  influx (Alavi and Cosson, 2006; Billard, 1986; Cosson et al.,  
79 2008; Morisawa, 2008; Takai and Morisawa, 1995) stimulated by hyper- or hypoosmotic  
80 shock after spawning into seawater or freshwater, respectively (Alavi and Cosson, 2006;  
81 Cherr et al., 2008; Krasznai et al., 2000; Morisawa, 2008; Vines et al., 2002). Therefore,  $\text{Ca}^{2+}$   
82 signalling in fish sperm must involve molecules different from those in marine invertebrates  
83 and mammals.

84 Second, the ionic milieu seriously constrains ion channel function. Sperm of freshwater fish,  
85 marine invertebrates, and mammals are facing entirely different ionic milieus.  $\text{K}^+$  and  $\text{Na}^+$   
86 concentrations in freshwater are extremely low (70  $\mu\text{M}$  and 200  $\mu\text{M}$ , respectively) compared  
87 to the orders-of-magnitude higher concentrations in seawater or the oviduct (Alavi and  
88 Cosson, 2006; Hugentobler et al., 2007). Furthermore,  $[\text{Ca}^{2+}]$  in seawater is high (10 mM),

89 whereas in freshwater it is low (< 1 mM). The low salt concentrations in freshwater probably  
90 require distinctively different ion channels. In fact, none of the ion channels controlling  
91 electrical excitation and Ca<sup>2+</sup> signalling of fish sperm are known.

92 Finally, fish sperm are not actively attracted to the whole egg from afar by chemical or  
93 physical cues, i.e. chemotaxis, thermotaxis, or rheotaxis (Cosson et al., 2008; Morisawa,  
94 2008; Yanagimachi et al., 2013). Instead, many fishes deposit sperm directly onto the eggs.  
95 For fertilization, sperm must search for the narrow entrance to a cone-shaped funnel in the  
96 egg coat – the micropyle – that provides access to the egg membrane. Sperm reach the  
97 micropyle probably by haptic interactions with tethered molecules that line the egg surface  
98 and the opening or interior of the micropyle (Iwamatsu et al., 1997; Ohta and Iwamatsu, 1983;  
99 Yanagimachi et al., 2013). At surfaces, sperm swim with their flagellum slightly inclined,  
100 which pushes the head against the wall and stabilizes sperm at the surface (Denissenko et al.,  
101 2012; Elgeti et al., 2010). Thus, fish sperm motility might be governed by specific  
102 hydrodynamic and haptic interactions with the egg surface and the micropyle.

103 Although the principal targets of a CNGK-mediated hyperpolarization – the Na<sup>+</sup>/H<sup>+</sup>  
104 exchanger and CatSper – are absent in fish, vertebrate orthologues of the sperm CNGK  
105 channel are present in various fish genomes (Figure 1 A). Here, we study the function of the  
106 CNGK channel in sperm of the freshwater fish *Danio rerio* (*DrCNGK*). The *DrCNGK*  
107 channel constitutes the principal K<sup>+</sup> channel in *D. rerio* sperm. Unexpectedly, cyclic  
108 nucleotides neither regulate CNGK channel activity nor sperm motility; instead, intracellular  
109 alkalization, a key mechanism to control sperm function in many species, strongly activates  
110 CNGK and, thereby, triggers a Ca<sup>2+</sup> signal and a motility response. Although its mechanism  
111 of activation is entirely different compared to sea urchin sperm, the principal CNGK function,  
112 namely to provide a hyperpolarization that triggers a Ca<sup>2+</sup> signal, is conserved. Our results

113 show that sperm signalling among aquatic species shows unique variations that probably  
114 represent adaptations to vastly different ionic milieus and fertilization habits.

115

## 116 **Results**

117 In several genomes, we identified genes encoding putative cyclic nucleotide-gated  $K^+$   
118 channels (CNGK) (Figure 1A). CNGK channels are primarily present in marine invertebrates,  
119 yet absent in the genomes of vertebrates such as birds, amphibians, and mammals, except  
120 freshwater fish and coelacanths. The CNGKs of freshwater fish appear to form a phylogenetic  
121 sub-group on their own (Figure 1A). Moreover, the CNGK channel exists in the unicellular  
122 choanoflagellate (*Salpingocea rosetta*), the closest living relative of animals (Levin and King,  
123 2013; Umen and Heitman, 2013).

124 CNGK channels feature a chimeric structure. Their overall four-repeat pseudotetrameric  
125 architecture is reminiscent of voltage-dependent  $Na_v$  and  $Ca_v$  channels, whereas the pore  
126 carries the canonical GYG or GFG motif of  $K^+$ -selective channels (Figure 1B and Figure 1-  
127 figure supplement 1). Furthermore, CNGK channels are phylogenetic cousins of cyclic  
128 nucleotide-gated (CNG) channels and of hyperpolarization-activated and cyclic nucleotide-  
129 gated (HCN) channels (Figure 1A); each of the four repeats harbours a cyclic nucleotide-  
130 binding domain (CNBD) (Figure 1B). In fact, the CNGK channel of sea urchin sperm is  
131 activated at nanomolar cGMP concentrations (Bönigk et al., 2009).

### 132 **Identification of a $K^+$ current in sperm of *D. rerio***

133 We recorded currents from whole *D. rerio* sperm (Figure 1-figure supplement 2, left panel) in  
134 the whole-cell patch-clamp configuration. Voltage steps from a holding potential of -65 mV  
135 evoked slightly inwardly rectifying currents (Figure 1C). Two pieces of evidence established  
136 that currents are carried by  $K^+$  channels and not by  $Cl^-$  channels. The reversal potential ( $V_{rev}$ )

137 shifted from  $-77 \pm 3$  mV ( $n = 18$ ) at 5.4 mM extracellular  $[K^+]_o$  to  $-7 \pm 1$  ( $n = 7$ ) mV at 140  
138 mM  $[K^+]_o$  ( $\Delta V_{rev} = 51 \pm 3$  mV/log  $[K^+]$ ,  $n = 7$ ) (Figure 1C, Figure1-figure supplement 3C).  
139 Changing the intracellular  $[Cl^-]$  did not affect  $V_{rev}$  (Figure1-figure supplement 3A,B). These  
140 results demonstrate that the current is predominantly carried by  $K^+$  ions. To localize the  
141 underlying  $K^+$  channel, we recorded currents from isolated sperm heads (Figure 1D-G, Figure  
142 1-figure supplement 2, middle panel). Head and whole-sperm currents displayed a similar  $K^+$   
143 dependence ( $\Delta V_{rev} = 52 \pm 2$  mV/log  $[K^+]$ ,  $n = 6$ ) (Figure 1D), rectification (Figure1F,G), and  
144 amplitude (Figure 1F,G), suggesting that the underlying  $K^+$  channel is primarily located in the  
145 head.

146 This result is unexpected, as ion channels involved in sperm signalling are usually localized to  
147 the flagellum. To test whether the *DrCNGK* channel is also localized to the head, we used  
148 Western blot analysis and immunocytochemistry. To this end, the *DrCNGK* protein was first  
149 characterized by heterologous expression in mammalian cell lines. *DrCNGK* constructs with  
150 a C-terminal HA-tag or with two tags, a C-terminal HA-tag and an N-terminal flag-tag, were  
151 expressed in CHOK1 cells (Figure 2A). In Western blots, the anti-HA-tag and the anti-flag-  
152 tag antibody labelled proteins of the same apparent molecular mass ( $M_w$ ) ( $173.9 \pm 3.9$  kDa  
153 ( $n = 13$ ) and  $175.4 \pm 4.0$  kDa ( $n = 3$ ), respectively) (Figure 2A). The  $M_w$  is smaller than the  
154 predicted  $M_w$  of 244.4 kDa. Because flag-tag and HA-tag antibodies recognized the N- and C-  
155 terminal end of the CNGK protein, respectively, we conclude that the 175-kDa band  
156 represents the full-length protein that, however, displays an abnormal electrophoretic mobility  
157 similar to other CNG channels (Körtschen et al., 1999; Körtschen et al., 1995).

158 We raised two antibodies against epitopes in repeat 1 and 3 of the *DrCNGK* protein (Figure  
159 1B, asterisks). Both antibodies labelled membrane proteins of about 170 kDa in Western blots  
160 of *DrCNGK*-expressing CHOK1 cells, *D. rerio* testis, and sperm, but not of heart, brain,  
161 ovaries, and eyes (Figure 2B,C). To scrutinize the antibody specificity, we analyzed by mass

162 spectrometry the ~170-kDa protein band from testis, mature whole sperm, isolated heads, and  
163 isolated flagella; 7, 23, 18, and 15 proteotypic *DrCNGK* peptides were identified, respectively  
164 (Figure 1-figure supplement 1, Figure 2-source data 1,2). Peptides covered almost the entire  
165 polypeptide sequence (Figure 1-figure supplement 1). The presence of *DrCNGK* in testis was  
166 confirmed by immunohistochemistry and *in situ* hybridization of *D. rerio* testis slices. The  
167 anti-repeat1 antibody labelled structures, most likely sperm, in the lumen of testicular  
168 compartments (Figure 2D, bottom left). An antisense RNA probe stained sperm precursor  
169 cells, in particular spermatocytes (Figure 2D, bottom right), but almost no primary or  
170 secondary spermatogonia.

171 Finally, the anti-repeat1 and anti-repeat3 antibodies intensely labelled the head and, to a lesser  
172 extent, the flagellum of single sperm cells (Figure 2E). In Western blots of isolated heads and  
173 flagella, the *DrCNGK* was readily identified in head preparations, yet was barely detectable in  
174 flagella preparations (Figure 2F, n = 4). In summary, the CNGK channel is located primarily  
175 in the head of mature *D. rerio* sperm.

#### 176 **The *DrCNGK* channel is not sensitive to cyclic nucleotides**

177 The sea urchin *ApCNGK* channel is opened by cyclic nucleotides and mediates the  
178 chemoattractant-induced hyperpolarization (Bönigk et al., 2009; Strünker et al., 2006).  
179 Unexpectedly, patch-clamp recordings of K<sup>+</sup> currents from *D. rerio* sperm required no cyclic  
180 nucleotides in the pipette (Figure 1C-G). Therefore, we scrutinized the action of cyclic  
181 nucleotides on sperm K<sup>+</sup> currents. Mean current amplitudes were similar in controls and in the  
182 presence of either cAMP or cGMP (100 μM) in the pipette solution (Figure 3 A). We used  
183 also caged cyclic nucleotides to study the K<sup>+</sup> current in the absence and presence of cyclic  
184 nucleotides in the same sperm cell (Kaupp et al., 2003). Photo-release of cAMP or cGMP  
185 from caged precursors did not affect K<sup>+</sup> currents, suggesting that cyclic nucleotides do not  
186 modulate *DrCNGK* (Figure 3B). In contrast, the photo-release of cAMP or cGMP induced a

187 rapid current increase in heterologously expressed cyclic nucleotide-gated channels *Ap*CNGK  
188 from sea urchin (Figure3-figure supplement 3A). We also heterologously expressed the  
189 *Dr*CNGK channel in *X. laevis* oocytes. The current-voltage (IV) relation (Figure 3C-F), K<sup>+</sup>  
190 dependence (Figure 3-figure supplement 1A-D), and block by external TEA (Figure 3-figure  
191 supplement 1E,F) was similar to that of the K<sup>+</sup> current recorded from *D. rerio* sperm.  
192 Moreover, currents in oocytes were also insensitive to the membrane-permeable analogs 8Br-  
193 cAMP and 8Br-cGMP (Figure 3C-F), whereas perfusion with 8Br-cGMP increased currents  
194 in oocytes that express the *Ap*CNGK channel from *A. punctulata* sperm (Figure 3-figure  
195 supplement 3B).

196 Membrane-permeant caged cyclic nucleotides have successfully been used to study sperm  
197 motility in sea urchin (Böhmer et al., 2005; Kashikar et al., 2012; Wood et al., 2005) and  
198 humans (Gakamsky et al., 2009). We studied *D. rerio* sperm motility before and after photo-  
199 release of cAMP (Figure 3G, left) or cGMP (Figure 3G, right) from caged precursors. The  
200 photo-release was followed by the increase of fluorescence of the free coumaryl cage  
201 (Figure3-figure supplement 5) (Bönigk et al., 2009). Swimming behaviour, i.e. path curvature  
202 (Figure 3H) and swimming speed (Figure 3-figure supplement 4A) were not altered by photo-  
203 release, showing that neither cAMP nor cGMP play a major role in the control of sperm  
204 motility. In conclusion, we observe no action of cyclic nucleotides on the *Dr*CNGK channel  
205 and on the swimming behaviour of *D. rerio* sperm.

206

### 207 **Rectification of CNGK channels in zebrafish and sea urchin sperm is different**

208 We noticed a much stronger rectification of currents carried by sea urchin *Ap*CNGK  
209 compared to zebrafish *Dr*CNGK (Figure 4A) and, therefore, investigated the origin of this  
210 pronounced difference. In classical K<sup>+</sup> channels, block by intracellular Mg<sup>2+</sup> (Matsuda et al.,

211 1987) or spermine (Fakler et al., 1995) produces inward rectification. However, neither  $Mg^{2+}$   
212 nor spermine affected *ApCNGK* rectification (Figure 4B). Instead, intracellular  $Na^+$  blocked  
213 outward currents in a strong voltage- and dose-dependent fashion (Figure 4B,D). In the  
214 absence of  $Na^+$ , the IV relation of *ApCNGK* and *DrCNGK* channels converged (Figure  
215 4A,B). We searched the pore regions of CNGK channels for clues regarding the molecular  
216 basis of the  $Na^+$  block. In three of the four *ApCNGK* pore motifs, we identified a Thr residue  
217 that in most  $K^+$  channels is replaced by a Val or Ile residue (Figure 4C). When these Thr  
218 residues were changed to Val, the strong rectification of the mutant *ApCNGK* channel was  
219 lost and the IV relation became similar to that of the *DrCNGK* channel (Figure 4E). We also  
220 tested the reverse construct, introducing Thr residues into the pore motif of *DrCNGK*  
221 channels. For unknown reasons, the mutants did not form functional channels.

222 Of note, the Thr residues are absent in CNGKs of freshwater organisms yet present in  
223 seawater organisms except for the sponge *AqCNGK* (Figure 4C), suggesting that the different  
224 CNGK pores represent adaptations to vastly different ionic milieus.

225

## 226 **The *DrCNGK* channel is controlled by intracellular pH**

227 Intracellular pH ( $pH_i$ ) is an important factor controlling sperm motility in marine invertebrates  
228 and mammals (Alavi and Cosson, 2005; Dziewulska and Domagala, 2013; Hirohashi et al.,  
229 2013; Lishko et al., 2010; Lishko and Kirichok, 2010; Nishigaki et al., 2014; Santi et al.,  
230 1998; Seifert et al., 2015). Moreover, in mouse sperm, the Slo3 channels and the CatSper  
231 channels are exquisitely pH-sensitive (Kirichok et al., 2006; Schreiber et al., 1998; Zeng et  
232 al., 2013; Zeng et al., 2011; Zhang et al., 2006a; Zhang et al., 2006b). Therefore, we  
233 examined whether *DrCNGK* is controlled by  $pH_i$ . At  $pH_i$  6.4, almost no CNGK current was  
234 recorded from *D. rerio* sperm (Figure 5A, left panel, B,C). To rule out that an increase of  $Ca^{2+}$

235 (from 91 pM to 7.7 nM, see materials and methods) due to the reduced buffering capacity of  
236 EGTA at pH 6.4 is responsible for current inhibition, we recorded sperm currents at pH 7.4  
237 with a free  $\text{Ca}^{2+}$  concentration of 1  $\mu\text{M}$  (Figure 5-figure supplement 2). Under these  
238 conditions, the  $\text{K}^+$  current in sperm was still large, indicating that protons and not  $\text{Ca}^{2+}$ , at  
239 least for the concentrations tested, are responsible for current inhibition. Exposing sperm to  
240 10 mM  $\text{NH}_4\text{Cl}$  rapidly elevates  $\text{pH}_i$  (Figure 5G), because  $\text{NH}_4\text{Cl}$  overcomes the buffer  
241 capacity of HEPES at pH 6.4 (Boron and De Weer, 1976; Seifert et al., 2015; Strünker et al.,  
242 2011). Alkaline  $\text{pH}_i$  strongly enhanced CNGK currents (Figure 5A, middle panel, B,C).  
243 Subsequent superfusion with 10 mM propionic acid, which lowers  $\text{pH}_i$ , completely reversed  
244 the  $\text{NH}_4\text{Cl}$ -induced CNGK currents (Figure 5A, right panel, B and C). The  $\text{NH}_4\text{Cl}$  action was  
245 very pronounced: 1 mM activated approximately 40% of the CNGK current; at 10 mM, the  
246 current was maximal (Figure 5D, triangles). To quantitatively determine the pH dependence,  
247 we recorded sperm  $\text{K}^+$  currents at different intracellular  $\text{pH}_i$  values (Figure 5C,D circles). The  
248 current is half-maximally activated at pH 7.08. The pH dependence allows to calibrate the  
249  $\text{NH}_4\text{Cl}$  action by superposing the data of the two different experimental conditions (Figure  
250 5D): For example, at an  $\text{NH}_4\text{Cl}$  concentration of 1.5 mM,  $\text{pH}_i$  in sperm will increase from 6.4  
251 to 7.08 (Figure 5D). Under current-clamp conditions, alkalization of *D. rerio* sperm with  
252 10 mM  $\text{NH}_4\text{Cl}$  evoked a rapid and reversible hyperpolarization from  $-49 \pm 7$  mV to  $-71 \pm$   
253  $4$  mV (Figure 5E,  $n = 10$ ). We also studied the pH regulation of the *DrCNGK* channel  
254 expressed in *Xenopus* oocytes. Oocytes were first perfused with a  $\text{K}^+$  bicarbonate solution,  
255 followed by a  $\text{K}^+$  gluconate-based solution including 1 mM  $\text{NH}_4\text{Cl}$  (Figure5-figure  
256 supplement 1). 1 mM  $\text{NH}_4\text{Cl}$  reversibly increased *DrCNGK* currents by approximately 71 %,  
257 demonstrating regulation by  $\text{pH}_i$  (Figure 5F). Higher concentrations of  $\text{NH}_4\text{Cl}$  further  
258 increased the *DrCNGK* current; however, these conditions also elicited significant currents in  
259 control oocytes, thus precluding quantitative analysis. Furthermore, we tested, whether  
260 *DrCNGK* channels in oocytes are activated by hypoosmotic conditions. Reducing the

261 osmolarity by ~50 % does not significantly change *DrCNGK* currents in oocytes (Figure 5-  
262 figure supplement 3, n = 4). In sea urchin sperm, CNGK-mediated hyperpolarization leads to  
263 an increase of intracellular  $\text{Ca}^{2+}$ . Therefore, we tested, whether the  $\text{NH}_4\text{Cl}$ -induced  
264 hyperpolarization (Figure 5E) and alkalization (Figure 5G) evokes a  $\text{Ca}^{2+}$  response. In fact,  
265 mixing of sperm with 10 or 30 mM  $\text{NH}_4\text{Cl}$  gave rise to a rapid  $\text{Ca}^{2+}$  signal (Figure 5H, n = 4).  
266 The time course of the  $\text{pH}_i$ - and  $\text{Ca}^{2+}$  signal was similar, suggesting that the CNGK-mediated  
267 hyperpolarization triggers a  $\text{Ca}^{2+}$  influx. We conclude that *DrCNGK* represents a pH-sensitive  
268 channel that is strongly activated at alkaline  $\text{pH}_i$ ; the ensuing hyperpolarization, like in sea  
269 urchin sperm, produces a  $\text{Ca}^{2+}$  signal.

270

#### 271 **$\text{Ca}^{2+}$ controls swimming behaviour of *D. rerio* sperm**

272 We studied the role of  $\text{Ca}^{2+}$  for motility of *D. rerio* sperm using photo-release of  $\text{Ca}^{2+}$  from  
273 caged  $\text{Ca}^{2+}$  (NP-EGTA). Sperm motility was activated by hypoosmotic dilution (1:20 into 70  
274 mM  $\text{Na}^+$  ES, 167 mOsm  $\times \text{L}^{-1}$ ) and was followed under a dark-field microscope (Figure 6,  
275 Movie 1). Unstimulated sperm swam on curvilinear trajectories of low curvature (Figure 6A-  
276 F, green segment, Video 1). A UV flash almost instantaneously increased path curvature in  
277 NP-EGTA-loaded sperm (Figure 6D-F,I), but not in control sperm (Figure 6A-C,I); sperm  
278 swam on much narrower arcs (Figure 6D-F, red segment, Video 1). The increase of path  
279 curvature was even more pronounced after a second UV flash (Figure 6 D-F, cyan segment, I,  
280 Video 1). Many cells were pushing against the wall of the observation chamber and  
281 performed a ‘spinning’ or ‘drilling’ behaviour, as if to penetrate the wall (Figure 6G). The  
282 asymmetry of the flagellar beat increased with each consecutive photo-release of  $\text{Ca}^{2+}$  and  
283 eventually the flagellum pointed away from the glass surface (Figure 6H, Video 1). This  
284 swimming behaviour likely represents a strategy followed by sperm on its search for the  
285 micropyle, a small opening (outer diameter about 8  $\mu\text{m}$  in diameter) (Hart and Danovan,

286 1983) on the surface of the much larger egg (about 0.75 mm in diameter) (Selman et al.,  
287 1993). A similar swimming behaviour during fertilization has been reported for sperm of  
288 herring and black flounder (Cherr et al., 2008; Yanagimachi et al., 2013; Yanagimachi et al.,  
289 1992). We propose that the spinning or drilling movements observed after  $\text{Ca}^{2+}$  release reflect  
290 the swimming behaviour *in vivo* down the narrow micropyle.

291

## 292 **Discussion**

293 A growing body of evidence reveals unexpected commonalities, but also notable differences  
294 among sperm from different species (for review (Darszon et al., 2006; Kaupp et al., 2008;  
295 Yoshida and Yoshida, 2011). Organisms, as phylogenetically distant as sea urchins and  
296 humans, share the CatSper channel as a common site of  $\text{Ca}^{2+}$  entry into the sperm flagellum.  
297 By the same token, Slo3  $\text{K}^+$  channel orthologues in mouse and human sperm evolved different  
298 selectivity for intracellular ligands and might serve different functions (Brenker et al., 2014;  
299 Chavez et al., 2013; Lishko et al., 2012; Santi et al., 2009; Zeng et al., 2013). Here, we  
300 characterize a novel variant of CNGK channels in zebrafish sperm, whose key features depart  
301 from those of CNGK channels of marine invertebrates (Figure 7).

302 First, although the *D. rerio* CNGK carries four canonical CNBDs, it is gated by  $\text{pH}_i$  rather  
303 than cyclic nucleotides, indicating that the CNBDs have lost their genuine ligand selectivity.  
304 The related *Ap*CNGK channel from sea urchin sperm is also unique in that it displays an  
305 unusual cGMP dependence: Unlike “classic” cooperative CNG channels, it is gated by  
306 binding of a single cGMP molecule to the third CNBD, implying that the other CNBDs are  
307 non-functional (Bönigk et al., 2009). Because the *Ap*CNGK channel is activated through  
308 binding of cGMP to the third repeat, we searched for sequence alterations in the third repeat  
309 of the *Dr*CNGK channel. Strikingly, in the C-linker region of the third repeat, we identified

310 an insert of 42 amino-acid residues (Figure 1-figure supplement 1, blue) that is absent in other  
311 cyclic nucleotide-regulated channels. The insert shows no sequence similarity to any known  
312 functional domain of ion channels. One hypothesis is that this insert prevents the transmission  
313 of the binding signal to the channel pore. Another sequence peculiarity is identified in the  
314 second repeat. At amino-acid position 934, an Ala residue replaces a highly conserved Arg  
315 residue that is crucial for cyclic-nucleotide binding (Kaupp and Seifert, 2002). The CNBDs of  
316 repeat 1 and 4 do not show obvious sequence abnormalities and could represent *bona fide*  
317 CNBDs. In recent years, many structures of CNBDs have been solved (Clayton et al., 2004;  
318 Kesters et al., 2015; Kim et al., 2007; Rehmman et al., 2003; Schünke et al., 2011; Schünke et  
319 al., 2009; Zagotta et al., 2003). Can we learn from these structures something about the  
320 *Dr*CNGK channel? Most of the CNBD structures feature a similar fold and are able to bind  
321 both cAMP and cGMP. However, for some CNG channels, ligands are full agonists, like  
322 cAMP and cGMP in the CNGA2 channel (Dhallan et al., 1990), only partial agonists, like  
323 cAMP in the CNGA1 channel (Altenhofen et al., 1991), or competitive antagonists, like  
324 cGMP in the bacterial SthK channel (Brams et al., 2014). Finally, in HCN channels, CNBDs  
325 interact and form a so-called gating ring (Zagotta et al., 2003), whereas in MloK1 channel,  
326 CNBDs do not interact at all (Cukkemane et al., 2007; Schünke et al., 2011; Schünke et al.,  
327 2009). In conclusion, at present, no sequence features can be identified that unequivocally  
328 explain the lack of cyclic-nucleotide regulation of the *Dr*CNGK channel.

329 The insensitivity of the *Dr*CNGK channel to cyclic nucleotides is, however, reminiscent of  
330 EAG and hERG channels that carry classic CNBDs, yet are not gated by cyclic nucleotides  
331 (Brelidze et al., 2010; Brelidze et al., 2012; Brelidze et al., 2009). Instead, small molecules  
332 such as flavonoids have been suggested as ligands that bind to the CNBD and modulate  
333 channel activity (Brelidze et al., 2010; Carlson et al., 2013). Moreover, in the C-terminus of  
334 these CNBDs, a conserved segment of residues was identified that occupies the CNBD and  
335 serves as an intrinsic “ligand” (Brelidze et al., 2012; Carlson et al., 2013). We can only

336 speculate, that, in addition to protons, as yet unidentified ligands might bind to and regulate  
337 the *DrCNGK* channel. The apparent  $pK_a$  value for channel activation by pH was  
338 approximately 7, suggesting that a His residue controls channel opening. There are a number  
339 of His residues in the C-linker of the four repeats that might serve as candidate sites. Future  
340 work is necessary to identify the site of pH regulation of the *DrCNGK* channel.

341 To take on a new ligand selectivity or activation mechanism is also reminiscent of  
342 orthologues of the sperm-specific  $K^+$  channel Slo3. Whereas the mouse Slo3 channel is  
343 exclusively controlled by  $pH_i$  (Brenker et al., 2014; Schreiber et al., 1998; Yang et al., 2011;  
344 Zeng et al., 2011; Zhang et al., 2006a), the human Slo3 is primarily regulated by  $Ca^{2+}$   
345 (Brenker et al., 2014). In conclusion, the zebrafish CNGK is a striking example for a channel  
346 featuring a CNBD that is not gated by cyclic nucleotides. In general, CNBDs might represent  
347 sensor domains that can relay information on ligands other than cyclic nucleotides.

348 Second, signalling pathways that control sperm motility are located to the flagellum: The GC  
349 receptor for chemoattractant binding in sea urchin (Bönigk et al., 2009; Pichlo et al., 2014),  
350 the CatSper channel in humans, mice, and sea urchin (Chung et al., 2014; Kirichok et al.,  
351 2006; Seifert et al., 2015), the Slo3  $K^+$  channel in mice and humans (Brenker et al., 2014;  
352 Navarro et al., 2007), and the HCN and the CNGK channel in sea urchin (Bönigk et al., 2009;  
353 Gauss et al., 1998). In contrast, the *DrCNGK* channel is located in the head rather than the  
354 flagellum. What might be the functional significance of such a peculiar location? The CNGK  
355 channel probably serves two related functions.

356 In seminal fluid, sperm of freshwater fish are immotile due to a high  $[K^+]$  and high  
357 osmolarity. Upon release into hypoosmotic freshwater, sperm become motile for a few  
358 minutes (Morisawa et al., 1983; Takai and Morisawa, 1995; Wilson-Leedy et al., 2009). The  
359 osmolarity-induced activation hyperpolarizes sperm and induces a  $Ca^{2+}$  signal (Krasznai et al.,  
360 2000). We propose that the CNGK triggers  $Ca^{2+}$  signalling events upon spawning: In the

361 high-K<sup>+</sup> seminal fluid, partially open CNGK channels keep sperm depolarized. When exposed  
362 to low-K<sup>+</sup> hypoosmolar conditions, sperm hyperpolarize and, ultimately, Ca<sup>2+</sup> is entering the  
363 cell and activates general motility (Figure 7).

364 Moreover, during the search for the micropyle on the egg surface, the sense of direction might  
365 be provided by haptic interaction with tethered molecules that line the opening or the funnel  
366 of the micropyle (Iwamatsu et al., 1997; Ohta and Iwamatsu, 1983; Yanagimachi et al., 2013).  
367 The haptic interactions could directly control CNGK activity in the head. For example, near  
368 or inside the micropyle, the CNGK might become further activated by alkaline pH and initiate  
369 the Ca<sup>2+</sup>-dependent ‘drilling’ behaviour.

370 On a final note, the study of zebrafish sperm provides insight into adaptive mechanisms of  
371 sperm evolution. Boundary conditions might constrain sperm to develop different signalling  
372 strategies for similar functions. One obvious constraint is the ionic milieu, which strongly  
373 affects ion channel function. In freshwater, ion concentrations are low and opening of Na<sup>+</sup>-,  
374 K<sup>+</sup>-, and non-selective cation channels would hyperpolarize rather than depolarize cells. We  
375 speculate that, in freshwater fish, a depolarization-activated Ca<sup>2+</sup> channel like CatSper may  
376 not work and has been replaced by another Ca<sub>v</sub> channel.

377 Furthermore, the Thr/Val difference in *ApCNGK* versus *DrCNGK*, which determines Na<sup>+</sup>  
378 blockage, probably represents an adaptation to the respective ionic milieu. Na<sup>+</sup> blockage of  
379 sea urchin CNGK resists hyperpolarization in seawater and, thereby, facilitates the opening of  
380 depolarization-activated CatSper channels. The observation that CNGK channels from  
381 seawater organisms carry this Thr residue indicates a specific evolutionary pressure on this  
382 pore residue. Why is this Thr residue lost in CNGK channels of freshwater organisms? We  
383 speculate that Na<sup>+</sup> blockage disappeared along with the loss of CatSper genes and that Ca<sup>2+</sup>  
384 ions enter fish sperm through a Ca<sup>2+</sup> channel that is activated by hyperpolarization rather than

385 depolarization. Future work needs to identify this Ca<sup>2+</sup> channel, its mechanism of activation,  
386 and its role for fertilization of teleost fish.

387 In summary, we identify a zebrafish CNGK channel that is activated at alkaline pH, and is set  
388 apart from its cousins of sea urchins that are activated by cGMP. Orthologues of CNGK also  
389 exist in the choanoflagellate *S. rosetta*, suggesting that this channel sub-family is  
390 phylogenetically ancient. Interestingly, this protozoon has a sexual life cycle: during  
391 anisogamous mating, small flagellated cells fuse with large cells (Levin and King, 2013). This  
392 mating behaviour represents the ancestor of sexual reproduction in animals (Levin and King,  
393 2013; Umen and Heitman, 2013). The role of the *S. rosetta* CNGK channel for sexual  
394 reproduction without sperm will be interesting to study.

395

## 396 **Materials and methods**

397

### 398 **Materials and reagents**

399 Chemicals were purchased from AppliChem, Biozym, Carl Roth, Fluka, GE Healthcare Life  
400 Sciences, Life Technologies, Merck, PolyScience, Qiagen, Serva, Sigma Aldrich, and Thermo  
401 Scientifica. Enzymes and corresponding buffer solutions were ordered from Ambion, MBI  
402 Fermentas, New England Biolabs, and Roche. Primers were synthesized from Eurofins  
403 Operon. Chemicals for mammalian cell culture were ordered from Carl Roth, Life  
404 Technologies, and Biochrom. CHOK1 and HEK293 cells were obtained from the American  
405 Type Culture Collection (ATCC).

### 406 **Cloning of the *DrCNGK* gene**

407 We identified two putative annotated sequences in the database: Eb934551 and XM\_0013354.  
408 Eb934551 contained the putative N-terminal region and XM\_0013354 contained the putative  
409 repeat 3, repeat 4, and parts of repeat 2. Using four sets of primer pairs, we did nested PCR  
410 reactions on testis cDNA to obtain the full-length sequence: the primer pairs #4811/#4812 and  
411 #4813/#4814 were used for XM\_0013354 and the primer pairs C0274/C0275 and  
412 C0276/C0277 for Eb934551. The primer sequences were: TATTTCAAGTAGCTGTTACCG  
413 (#4811), ACATTCCTTATAATAATGTCC (#4812),  
414 AAAAAAGCTAAGCTTTTCAGAAACACAG (#4813),  
415 AAAATCTGACAGGTACCCTGCAGAATGC (#4814), CATA CAGGATGCATGACCCC  
416 (C0274), CCAGGAATGTATGTGTAGGTC (C0275),  
417 GAGGAATTCATGCATGACCCCAGAGAAATGAAG (C0276) and  
418 CTCGGATCCGTATGTGTAGGTCTTTAATTCAGGG (C0277). Due to failure of  
419 expression, we used a codon-optimized version (human codon usage) of the *DrCNGK* gene  
420 separated into three modules (Eurofins MWG Operon). Each module was flanked by  
421 restriction sites. The first module contained bases 1 to 2,108 and was flanked on the 5' end  
422 with BamHI and on the 3' end with XbaI; the second module contained bases 2,109 to 4,655  
423 and was flanked on the 5' end with XbaI and on the 3' end with EcoRI; the third module  
424 contained bases 4,656 to 6,360 and was flanked on the 5' end with EcoRI and on the 3' end  
425 with NotI. At the 3' end, the coding sequence for the hemagglutinin tag (HA-tag) was added.  
426 The construct was cloned into the pcDNA3.1 vector (Life technologies) (*DrCNGK*). To  
427 enhance expression levels, we added a QBI SP163 sequence (Stein et al., 1998) in front of the  
428 start codon (QBI-*DrCNGK*).

429 Moreover, we added the coding sequence for a flag-tag at the 5' end of the *DrCNGK* gene.  
430 We performed two PCR reactions with primer pairs C0991/C0962 and C0417/C0990 and a  
431 recombinant PCR reaction on the resulting PCR products with primer pair C0417/C0962.  
432 Primer sequences were:

433 CCCGGACGGCCTCCGAAACCATGGACTACAAGGACGACGACGACAAGC (C0991),  
434 TTCAGACCGGCATTCCAAGCCC (C0962),  
435 CGCGGATCCAGCGCAGAGGCTTGGGGCAGC (C0417),  
436 GTCGTCGTCGTCCTTGTAGTCCATGGTTTCGGAGGCCGTCCGGG (C0990).

437 *Ap*CNGK pore mutants: for the pore mutant *Ap*CNGK-4V, the following amino-acid  
438 substitutions in the *Ap*CNGK wild-type channel (Bönigk et al., 2009) were produced: T252V,  
439 T801V and T1986V. Three PCR reactions were required for each mutation: two with the  
440 primers containing the point mutation and one recombinant PCR reaction. For the amino-acid  
441 exchange T252V, the primer pairs #4433/C0531 and C0530/#4409 were used and for the  
442 recombinant PCR, the primer pair #4433/#4409. The PCR product was cloned into the  
443 *Ap*CNGK gene with restriction enzymes BamHI and XhoI. For the amino-acid exchange  
444 T802V, primer pairs #4436/C0533 and C0532/#4439 were used and for the recombinant PCR  
445 the primer pair #4436/#4439. The PCR product was cloned into the *Ap*CNGK gene with  
446 restriction enzymes XhoI and XbaI. For the amino-acid exchange T1986V, the primer pairs  
447 #4412/C0535 and C0534/#4447 were used and for the recombinant PCR, the primer pair  
448 #4412/#4447. The PCR product was cloned into the *Ap*CNGK gene with restriction enzymes  
449 BamHI and XbaI. The primer sequences were: GGTTCTGCTCGAGATTCTGTAGG  
450 (#4409), CAACACCGGATCCGGTGAGAGCAGTG (#4412),  
451 AAAGTTGGGATCCAATACAGCG (#4433), TACAGAATCTCGAGCAGAACC (#4436),  
452 AAGTCTAGACGGTAGACTGATCGCCTGG (#4439),  
453 AAATCTAGATTAGGCATAATCGGGCACATCATAGGGATACACCACCGTTTGTCTC  
454 AGCG (#4447), GCCACCTCTGTAGGCTACGGAGAC (C0530),  
455 GTCTCCGTAGCCTACAGAGGTGGC (C0531), ATGACATCCGTGGGCTACGGAGAC  
456 (C0532), GTCTCCGTAGCCCACGGATGTCAT (C0533),  
457 CTGACCTCCGTTGGCTACGGTGACATC (C0534),  
458 GTCACCGTAGCCAACGGAGGTCAGAG (C0535).

459 For expression in *X. laevis* oocytes, the *DrCNGK* and *QBI-DrCNGK* constructs were cloned  
460 into a modified version of the expression vector pGEMHEnew (Liman et al., 1992); because  
461 cloning of *DrCNGK* was only possible using BamHI and NotI, a NotI restriction site present  
462 in pGEMHEnew was removed and a new one was introduced into the multiple-cloning site.  
463 This new vector has been named pGEMHEnew-NotI. *In vitro* transcription to generate cRNA  
464 was performed using the mMESSAGEMMACHINEKit (Ambion); the plasmid was linearized  
465 with SpeI.

466 For *in situ* hybridization, a short fragment of the *DrCNGK* gene coding for amino acids  
467 1,085-1,219 was cloned into the pBluescript vector using PstI and HindIII. Nested PCR  
468 reactions were performed using for the 1<sup>st</sup> reaction the primer pair #4791/#4792 and for the  
469 2<sup>nd</sup> reaction the primer pair #4793/#4794. Primer sequences were:  
470 ATTTTGCCGTGGAGTCCATGG (#4791), AAGTCAATATTAACGTTGCATCC  
471 (#4792), GGAAGCTTCCGAAGCATTACAGCCG (#4793),  
472 GTTGGATCCAAGTGTGTCACCCATGAC (#4794). For the antisense probe, the plasmid  
473 was linearized with HindIII and transcribed by T7 RNA polymerase. RNA was labeled with  
474 Digoxigenin (DIG RNA Labelling Mix, Roche).

#### 475 **Preparation of testis, sperm, heads and flagella**

476 Animals were sacrificed according to the “Guidelines for housing and care, transport, and  
477 euthanasia of laboratory fishes”, (“Empfehlung für die Haltung, den Transport und das  
478 tierschutzgerechte Töten von Versuchsfischen”, published by the Tierärztliche Vereinigung  
479 für Tierschutz e.V. January 2010). To obtain intact sperm, zebrafish male were anesthetized  
480 with MS-222 (0.5 mM, 3 min). After a brief wash with fresh water, the head was quickly  
481 separated from the body. The body of the fish was ventrally opened and two testis strands  
482 were removed and transferred into ES buffer (see electrophysiology) or phosphate-buffered  
483 saline (PBS) containing (in mM: NaCl 137, KCl 2.7, Na<sub>2</sub>HPO<sub>4</sub> 6.5, KH<sub>2</sub>PO<sub>4</sub> 1.5, pH 7.4),

484 additionally containing 1.3 mM EDTA, mPIC protease inhibitory cocktail (Sigma), and 1 mM  
485 DTT. Sperm were collected with a pipette tip. After 15 min, 80% of the supernatant was  
486 transferred into a fresh reaction tube. To separate heads from flagella, the sperm suspension  
487 was sheared 30-40 times on ice with a 24 gauge needle. The sheared suspension was  
488 centrifuged for 10 min (800xg, 4 °C) to sediment intact sperm and sperm heads. This  
489 procedure was repeated twice. The purity of flagella preparations was assessed using dark-  
490 field microscopy (Figure 1-figure supplement 2). For testis sections, males were ventrally  
491 sliced and kept overnight in 4% paraformaldehyde. After 24 h, testis strands were removed  
492 and embedded in paraffin. Sections (8 µm) were made using a microtome (Leica).

### 493 **Primary antibodies**

494 A rabbit polyclonal antibody produced by Peptide Specialty Laboratories (PSL, Heidelberg)  
495 was directed against the cytosolic loop C-terminal of the CNBD of the first repeat (anti-  
496 repeat1, amino acids 483 - 497). Antibodies were purified with a peptide affinity column  
497 provided by PSL. Rat monoclonal antibody YENT1E2 (anti-repeat3) was directed against the  
498 extracellular loop between S5 and the pore region of the third repeat (amino acids 1,254 -  
499 1,269). Anti- $\alpha$ -tubulin (mouse, B-5-1-2, Sigma), anti- $\beta$ -actin (mouse, abcam), anti-HA (rat,  
500 3F10, Roche), anti-calnexin (rabbit, abcam), and anti-flag-tag (mouse, M2, Sigma) antibodies  
501 were used as controls.

### 502 **Immunocytochemistry, *in situ* hybridization, and Western blot analysis**

503 Sperm were immobilized on SuperFrost Plus microscope slides (Menzel) and fixed for 5 min  
504 with 4% paraformaldehyde. After preincubation with 0.5% Triton X-100 and 5%  
505 chemiblocker (Millipore) in PBS, sperm were incubated for 1 hour with antibodies YENT1E2  
506 (1:10) or anti-repeat1 (1:500) diluted in 5% chemiblocker (Millipore) and 0.5% TritonX-100

507 in PBS (pH 7.4). Sperm were visualized with Cy3-conjugated secondary antibody (Jackson  
508 ImmunoResearch Laboratories).

509 For *in situ* hybridization, tissue was permeabilized with protein kinase K (1 µg/ml in 0.1 M  
510 Tris/HCl, pH 8.0) and hybridized using the *Dr*CNGK-3 antisense probe. After washing, the  
511 antibody staining was performed using an anti-Digoxigenin antibody (1:500, Roche)  
512 conjugated with alkaline phosphatase. RNA was visualized with a mixture of nitro-blue  
513 tetrazolium chloride (500 µg) and 5-bromo-4-chloro-3'-indolyphosphate p-toluidine salt (188  
514 µg, Roche). Cross sections were covered with a glass slip. For antibody staining of the *in situ*  
515 hybridization sections, cover slips were removed keeping the slides 5 min in xylene and  
516 briefly in PBS. This step was repeated; the fixative was removed from the sections.  
517 Afterwards, sections were stained as described for sperm immunocytochemistry. Proteins  
518 were probed with antibodies: anti-repeat1 (1:500) or anti-repeat3 (1:10) and visualized with  
519 Cy3-conjugated secondary antibody (Jackson ImmunoResearch Laboratories).

520 For Western blotting, zebrafish tissue or cells heterologously expressing the *Dr*CNGK  
521 channel were resuspended in PBS buffer containing 1.3 mM EDTA, mPIC protease inhibitor  
522 cocktail (Sigma), and 1 mM DTT. For lysis, cells were triturated 20x with a cannula (24G,  
523 Braun) and sonicated three times for 15 s. After a clearing spin (25,000xg, 30 min, 4 °C), the  
524 pellet was resuspended and sonicated two times for 10 s in 200 mM NaCl, 50 mM Hepes (pH  
525 7.5), mPIC, and 1 mM DTT. Triton X-100 was added to a final concentration of 1%. Proteins  
526 were solubilized for 1-2 h at 4 °C. A final clearing spin (10,000xg, 20 min, 4 °C) was  
527 performed. For Western blot analysis, proteins were separated using 4-12% NuPAGE gradient  
528 gels (Life Technologies) and transferred overnight (4 °C, 12 - 15 V) onto PVDF membranes  
529 (Immobilion FL, Millipore), using a Xcell SureLock minigel chamber (Life Technologies).  
530 Membranes were incubated with Odyssey blocking buffer (LI-COR Biosciences). Proteins  
531 were probed with the following antibodies: anti-repeat1 (1:1,000), anti-repeat3 (1:10), anti- $\alpha$ -  
532 tubulin (1:2,000), anti- $\beta$ -actin (1:1,000), anti-HA (1:1,000), anti-calnexin (1:5,000), and anti-

533 flag-tag (1:200). Proteins were visualized using IRDye800CW-conjugated secondary  
534 antibodies (1:10,000, LI-COR Biosciences), IRDye680-conjugated secondary antibodies  
535 (1:10,000, LI-COR Biosciences), or horseradish peroxidase-conjugated secondary antibodies  
536 (1:5,000, Jackson ImmunoResearch Laboratories). Visualization took place either with a  
537 chemiluminescence detection system (LAS-3000 Luminescent Image Analyzer, FUJIFILM)  
538 or with fluorescent secondary antibodies (Odyssey infrared imaging system). The Novex  
539 Sharp pre-stained protein standard (Life Technologies) was used as molecular mass standard.

#### 540 **Electrophysiology**

541 We electrically recorded from intact zebrafish sperm and from isolated sperm heads using the  
542 patch-clamp technique in the whole-cell configuration. Recordings were accomplished within  
543 4 hours after preparation. Seals between pipette and sperm were formed at the neck region in  
544 standard extracellular solution (ES). The following pipette solutions were used: standard  
545 intracellular solution (IS) (in mM): NaCl 10, K<sup>+</sup> aspartate 130, MgCl<sub>2</sub> 2, EGTA 1, Na<sub>2</sub>ATP 2,  
546 and Hepes 10 at pH 8.4, 7.9, 7.4, 6.9, or 6.4 adjusted with KOH; Cl<sup>-</sup>-based IS (in mM): NaCl  
547 10, KCl 130, MgCl<sub>2</sub> 2, EGTA 1, Na<sub>2</sub>ATP 2, and Hepes 10 at pH 7.4 adjusted with KOH. The  
548 following bath solutions were used: standard ES (in mM): NaCl 140, KCl 5.4, MgCl<sub>2</sub> 1,  
549 CaCl<sub>2</sub> 1.8, glucose 10, and Hepes 5 at pH 7.4 adjusted with NaOH; for K<sup>+</sup>-based ES solutions,  
550 the equivalent amount of Na<sup>+</sup> was replaced by K<sup>+</sup> (concentrations are indicated in the Figure  
551 legends). Calculations of the free Ca<sup>2+</sup> concentrations were carried out using the Maxchelator  
552 program (<http://maxchelator.stanford.edu/webmaxc/webmaxcE.htm>) assuming a residual Ca<sup>2+</sup>  
553 concentration in water of 1 μM. At pH 6.4, [Ca<sup>2+</sup>]<sub>i</sub> was 7.7 nM and at pH 7.4, it was 91 pM.  
554 To obtain an intracellular solution with 1 μM free Ca<sup>2+</sup>, 1 mM CaCl<sub>2</sub> was added to the IS  
555 solution at pH 7.4.

556 Caged compounds (100 μM BCMACM-caged cAMP or 100 μM BCMACM-caged cGMP)  
557 were added to the IS. The final concentration of DMSO was 0.1%. The compounds were

558 photolyzed by a ~1 ms flash of ultraviolet light from a Xenon flash lamp (JML-C2; Rapp  
559 OptoElectronic). The flash was passed through a BP295-395 nm filter (Rapp OptoElectronic)  
560 and delivered to the patch-clamp chamber in the microscope by a liquid light guide. Pipette  
561 resistance in IS/ES was between 11.5 and 15.0 MΩ. Voltages were corrected for liquid  
562 junction potentials.

563 For functional studies in *X. laevis* oocytes, 50 nl *DrCNGK* RNA (0.3, 0.4, and 0.6 μg/μl) per  
564 oocyte were injected. Oocytes were purchased from EcoCyte Bioscience or prepared from  
565 dissected animals. Briefly, frogs were anesthetized with MS-222 (0.5%, 10-20 min), follicles  
566 were removed, opened with forceps and washed several times with ND96 solution. For  
567 defolliculation, oocytes were transferred for 1-2 hrs (RT) into Ca<sup>2+</sup>-free OR-2 solution  
568 containing 3 mg/ml collagenase type IV (Worthington). Defolliculated oocytes were stored  
569 in ND96 solution containing (in mM): NaCl 96, KCl 2, MgCl<sub>2</sub> 1, CaCl<sub>2</sub> 1.8, Hepes 10 at pH  
570 7.6, pyruvate 2.5, and gentamycin 1. The OR-2 solution contained (in mM): NaCl 82.5, KCl  
571 2.5, MgCl<sub>2</sub> 1, Hepes 5 at pH 7.6. We recorded in the Two-Electrode Voltage-Clamp  
572 configuration. Most data were recorded with a Dagan Clampator One (CA-1B) amplifier and  
573 digitized with Digidata 1320A (Axon Instruments). Analogue signals were sampled at 2 kHz.  
574 The holding potential was -80 mV. Pipette solution: 3 M KCl. Bath solutions were ND96-7K  
575 (in mM): NaCl 96, KCl 7, MgCl<sub>2</sub> 1, CaCl<sub>2</sub> 1.8, Hepes 10 at pH 7.4 adjusted with NaOH; K<sup>+</sup>-  
576 based solution K96-7Na (in mM): NaCl 7, KCl 96, MgCl<sub>2</sub> 1, CaCl<sub>2</sub> 1.8, Hepes 10 at pH 7.4  
577 adjusted with KOH. Recordings with reduced osmolarity were carried out in ND48-7K  
578 solution (in mM): NaCl 48, KCl 7, CaCl<sub>2</sub> 1.8, MgCl<sub>2</sub> 1, HEPES 10 at pH 7.4 adjusted with  
579 NaOH. Pipette resistance of voltage electrodes ranged between 1.5 and 3.0 MΩ and of current  
580 electrodes between 0.5 and 1.5 MΩ. Different analogues of cyclic nucleotides were added to  
581 the bath solution as indicated. Oocytes recordings with bicarbonate-based solutions were  
582 performed at Stanford University. Data were recorded with an OC-725C amplifier (Warner  
583 Instruments) using Patchmaster (HEKA Elektronik) as acquisition software. Analogue signals

584 were sampled at 1 kHz. The holding potential was -60 mV. Pipette solutions and pipette  
585 resistance as described above. Bath solutions: K<sup>+</sup> bicarbonate-based solution (in mM): NaCl  
586 7, K-bicarbonate 96, MgCl<sub>2</sub> 1, CaCl<sub>2</sub> 1.8, Hepes 5 at pH 7.65. Solution was made fresh on  
587 each day of recording; K<sup>+</sup> gluconate-based solution (in mM): NaCl 7, K-gluconate 96, MgCl<sub>2</sub>  
588 1, CaCl<sub>2</sub> 1.8, Hepes 5 at pH 7.65 adjusted with KOH. NH<sub>4</sub>Cl was dissolved in K<sup>+</sup> gluconate-  
589 based solution.

590 We recorded *ApCNGK* and mutant *ApCNGK* currents from transfected (Lipofectamine 2000,  
591 Life technologies) HEK293 cells with the patch-clamp technique in the whole-cell  
592 configuration. A HEK293 cell line stably expressing the *ApCNGK* channel was used for  
593 inside-out recordings. The pipette solution for whole-cell recordings was standard IS.  
594 Channels were activated with 100 μM cGMP. The pipette solution for inside-out recordings  
595 was standard ES. The following bath solutions were used for inside-out recordings: IS-30  
596 NMDG-0Na<sup>+</sup> solution (in mM): NaCl 0, NMDG 30, KCl 110, EGTA 0.1, Hepes 10 at pH 7.4  
597 adjusted with KOH; IS-NMDG-30Na<sup>+</sup> solution (in mM): NaCl 30, KCl 110, EGTA 0.1,  
598 Hepes 10 at pH 7.4 adjusted with KOH. 30 NMDG-0Na<sup>+</sup> and 0NMDG-30Na<sup>+</sup> solutions were  
599 mixed to obtain the desired Na<sup>+</sup> concentrations. 100 μM Na<sup>+</sup>-cGMP was added to the bath  
600 solution. For the solution with 0 mM Na<sup>+</sup>, we used 100 μM Na<sup>+</sup>-free cGMP. Pipette resistance  
601 in IS/ES was between 4.0 and 7.0 MΩ.

## 602 **Measurement of changes in intracellular Ca<sup>2+</sup> concentration and pH**

603 We measured changes in [Ca<sup>2+</sup>]<sub>i</sub> and pH<sub>i</sub> in a rapid-mixing device (SFM-4000; BioLogic) in  
604 the stopped-flow mode using the Ca<sup>2+</sup> indicator Cal-520-AM (AAT Bioquest) or the pH  
605 indicator BCECF-AM (Invitrogen). All sperm from a zebrafish male were diluted into 100 μl  
606 of ES solution and incubated with either 10 μM Cal-520-AM and 0.5% Pluronic for 120-  
607 180 min or 10 μM BCECF-AM for 10 min. Sperm were washed once, diluted 1:20 into ES  
608 solution, and loaded into the stopped-flow device. The sperm suspension was rapidly mixed

609 1:1 (vol/vol) with control ES solution or with ES solution containing NH<sub>4</sub>Cl to obtain final  
610 concentrations of 10 mM and 30 mM after mixing. Fluorescence was excited by a SpectraX  
611 Light Engine (Lumencor). Cal-520 was excited with a 494/20 nm (Semrock), BCECF with a  
612 452/45 nm (Semrock) excitation filter. Emission was recorded by photomultiplier modules  
613 (H9656-20; Hamamatsu Photonics). Fluorescence of Cal-520 was recorded using a 536/40 nm  
614 (Semrock) emission filter and normalized (without background subtraction) to the value  
615 before stimulation. BCECF fluorescence was recorded in the dual emission mode using a  
616 494/20 nm (Semrock) and a 549/15 nm (Semrock) emission filter. The pH<sub>i</sub> signals represent  
617 the ratio of F<sub>494/549</sub> and were normalized (without background subtraction) to the value  
618 before stimulation. All stopped-flow traces represent the average of 3-6 recordings. The  
619 signals were normalized to the first 5-10 data points before the onset of the signal to yield  
620  $\Delta F/F$  and  $\Delta R/R$ , respectively.

621

## 622 **Mass spectrometric identification of the *DrCNGK* channel**

623 Proteins of whole sperm, isolated heads, or flagella were resuspended in SDS sample buffer  
624 and loaded on a SDS gel; after proteins had migrated approximately 1 cm into the separation  
625 gel, the gel was stained with Coomassie. The single gel band was excised for every sample,  
626 and proteins were in-gel digested with trypsin (Promega, USA); peptides were separated by  
627 RP-LC (180 min gradient 2-85% acetonitrile, (Fisher Scientific, USA)) using a nanoAcquity  
628 LC System (Waters, USA) equipped with a HSS T3 analytical column (1.8  $\mu$ m particle, 75  
629  $\mu$ m x 150 mm) (Waters, USA) and analyzed twice by ESI-LC-MS/MS, using an LTQ  
630 Orbitrap Elite mass spectrometer (Thermo, USA) with a 300-2,000 m/z survey scan at  
631 240,000 resolution, and parallel CID of the 20 most intense precursors from most to least  
632 intense (top20) and from least to most intense (bottom20) with 60 s dynamic exclusion. All  
633 database searches were performed using SEQUEST and MS Amanda algorithm (Dorfer et al.,

634 2014), embedded in Proteome Discoverer<sup>TM</sup> (Rev. 1.4, Thermo Electron<sup>©</sup> 2008-2011), with  
635 both a NCBI (26,623 entries, accessed December 20th, 2010) and a Uniprot (40,895 entries,  
636 accessed April 24th, 2014) zebrafish sequence protein database, both supplemented with the  
637 *DrCNGK* protein sequence (Figure 1-figure supplement 2). Only peptides originating from  
638 protein cleavage after lysine and arginine with up to two missed cleavages were accepted.  
639 Oxidation of methionine was permitted as variable modification. The mass tolerance for  
640 precursor ions was set to 8 ppm; the mass tolerance for fragment ions was set to 0.6 amu. For  
641 filtering of search results and identification of *DrCNGK*, a peptide FDR threshold of 0.01 (q-  
642 value) according to Percolator (Käll et al., 2007) two unique peptides per protein and peptides  
643 with search result rank 1 were required.

#### 644 **Sequence analysis**

645 Alignments for the calculation of the phylogenetic tree were done with ClustalOmega. Tree  
646 was depicted with Tree view (Page, 1996). The following ion channel sequences were used  
647 for the phylogenetic tree: CNGK channels from zebrafish (*Danio rerio*, *DrCNGK*,  
648 XP\_001335499.5); rainbow trout (*Oncorhynchus mykiss*, *OmCNGK*, CDQ79437.1); spotted  
649 gar (*Lepisosteus oculatus*, *LoCNGK*, W5MTF2); West Indian ocean coelacanth (*Latimeria*  
650 *chalumnae*, *LcCNGK*, H3BE11); sea urchin (*Arbacia punctulata*, *ApCNGK*); acorn worm  
651 (*Saccoglossus kowalevskii*, *SkCNGK*, XP\_002731383.1); amphioxus (*Branchiostoma*  
652 *floridae*, *BfCNGK*, XP\_002592428.1); starlet sea anemone (*Nematostella vectensis*,  
653 *NvCNGK*, XP\_001627832); vasa tunicate (*Ciona intestinalis*, *CiCNGK*, XP\_002123955);  
654 sponge (*Amphimedon queenslandica*, *AqCNGK*, I1G982); choanoflagellate (*Salpingoeca*  
655 *rosetta*, *SrCNGK*, XP\_004992545.1); murine HCN channel 1 (*Mus musculus*, *mHCN1*,  
656 NP\_034538), 2 (*mHCN2*, NP\_032252), 3 (*mHCN3*, NP\_032253.1), and 4 (*mHCN4*,  
657 NP\_001074661), and the HCN channel from sea urchin (*Strongylocentrotus purpuratus*,  
658 *SpHCN1*, NP\_999729); rat cyclic nucleotide-gated channels *CNGA1* (*Rattus rattus*,

659 *r*CNGA1, NP\_445949), A2 (*r*CNGA2, NP\_037060), A3 (*r*CNGA3, NP\_445947.1), and A4  
660 (*r*CNGA4, Q64359); the KCNH channels from fruit fly (*Drosophila melanogaster*, *DmEAG*,  
661 AAA28495) and human (*Homo sapiens*, *hERG*, BAA37096.1); murine voltage-gated Na<sub>v</sub>  
662 channels (*Mus musculus*, *mNa<sub>v</sub> 1.1*, NP\_061203 and *mNa<sub>v</sub> 1.6*, NM\_001077499.2); murine  
663 voltage-gated Ca<sub>v</sub> channels (*Mus musculus*, *mCa<sub>v</sub>1.1*, NP\_055008, *mCa<sub>v</sub>2.3*, NP\_033912.2,  
664 and *mCa<sub>v</sub>3.1*, NP\_033913.2); and voltage-gated K<sub>v</sub> channels from fruit fly (*Drosophila*  
665 *melanogaster*, *DmShaker*, CAA29917.1) and mouse (*Mus musculus*, *mK<sub>v</sub>3.1*,  
666 NM\_001112739.1).

### 667 **Sperm motility**

668 Sperm were loaded for 45 min at room temperature with either 30 μM DEACM-caged cAMP,  
669 30 μM DEACM-caged cGMP, or 40 μM caged Ca<sup>2+</sup> (NP-EGTA, Life Technologies). A UV  
670 light-emitting diode (365-nm LED; M365L2-C, Thorlabs) was used for photolysis of caged  
671 compounds. Experiments using caged Ca<sup>2+</sup> and DEACM-caged nucleotides were carried out  
672 using a UV power of 25 and 22 mW, respectively. Flash duration was 300 ms. Pluronic  
673 (0.5%) was added to the incubation solution. Sperm were kept quiescent during incubation in  
674 ES solution (292 mOsm x L<sup>-1</sup>). Swimming was initiated by a hypoosmotic shock diluting  
675 sperm 1:20 in an activation solution containing (in mM): NaCl 70, KCl 5.4, MgCl<sub>2</sub> 1, CaCl<sub>2</sub>  
676 1.8, glucose 10, and Hepes 5 at pH 7.4 adjusted with NaOH (167 mOsm x L<sup>-1</sup>). Swimming  
677 behaviour was observed with a dark-field condenser in an inverse microscope (IX71,  
678 Olympus) with 20x magnification (UPLSAPO, NA 0.75). Movies were recorded at 30 Hz  
679 using a back-illuminated electron-multiplying charge-coupled device camera (DU-897D;  
680 Andor Technology). Sperm trajectories were tracked using custom-made software written in  
681 MATLAB (Mathworks). The software can be made available upon request. The average  
682 swimming path (ASP) was calculated by filtering the tracked coordinates with a second

683 degree Savitzky-Golay filter with a 200 ms span. The curvature ( $\kappa$ ) of the swimming path was  
684 calculated using the formula:bbb

685  $\kappa = \left( \frac{\dot{x}\dot{y} - \dot{y}\dot{x}}{\dot{x}^2 + \dot{y}^2} \right)^{3/2}$ , where  $x$  and  $y$  are the coordinates of the ASP.

686 To assess cAMP loading and release, we recorded the fluorescence increase due to DEACM-  
687 OH release after photolysis of DEACM-caged cAMP (Bönigk et al. 2009). Release and  
688 fluorescence excitation was achieved simultaneously using the same UV LED (power 1.75  
689 mW). Light was coupled to the microscope with a dichroic mirror (455DRLP, XF2034,  
690 Omega Optical) and fluorescence was long-pass filtered (460ALP; XF309; Omega Optical).  
691 Single cells were recorded at 50 Hz.

692

693

694 **Data analysis** Statistical analysis and fitting of data were performed, unless otherwise stated,  
695 using Sigma Plot 11.0, GraphPadPrism 5, or Clampfit 10.2 (Molecular Devices). All data are  
696 given as mean  $\pm$  standard deviation (number of experiments).

697

698 **Note:** All cell lines used in this study will be sent for STR profiling. Mycoplasma testing was  
699 performed using the Promokine Mycoplasma Test Kit 1/C (PromoCell GmbH, Heidelberg).  
700 Results of this test can be supplied upon request.

701

702 **Acknowledgements** We thank Drs. K. Benndorf, and J. Kusch (University Jena) and Drs. E.  
703 Miranda-Laferte and P. Hidalgo (Research Center Jülich), and Dr. M Goodman (Stanford  
704 University) for support with oocyte expression and H. Krause for preparing the manuscript.  
705 S.F. was a fellow of the Boehringer Ingelheim Fonds. The authors declare no competing  
706 financial interests.

707

708 **Author Contributions** S.F., R.S., and U.B.K. designed the project and experiments. S.F.,  
709 R.S., and T.B. performed electrophysiological experiments, S.F. performed biochemical and  
710 cell biology experiments. S.F. and R.S. performed stopped-flow experiments. K.R.S.  
711 performed in situ hybridization. C.T. and A.P. performed the MS analysis; S.F., R.P., and  
712 L.A. performed motility experiments and analysis. W.B. and A.M. cloned the CNGK gene  
713 and mutants. S.F. and G.S. performed the oocyte experiments. E.K. produced the monoclonal  
714 antibodies. U.B.K., R.S., L.A., and S.F. wrote the manuscript. All authors read and corrected  
715 the manuscript.

716

717 **Competing financial interests** The authors declare no competing financial interests

718

719

720

721

#### References

722

723 Alavi SM Cosson J. 2005. Sperm motility in fishes. (I) Effects of temperature and pH: a review. *Cell Biol. Int.*  
724 **29**:101-110. 10.1016/j.cellbi.2004.11.021

725

726 Alavi SM Cosson J. 2006. Sperm motility in fishes. (II) Effects of ions and osmolality: a review. *Cell Biol. Int.*  
727 **30**:1-14. 10.1016/j.cellbi.2005.06.004

728

729 Altenhofen W, Ludwig J, Eismann E, Kraus W, Bönigk W Kaupp UB. 1991. Control of ligand specificity in  
730 cyclic nucleotide-gated channels from rod photoreceptors and olfactory epithelium. *Proc. Natl. Acad. Sci. USA*  
731 **88**:9868-9872.

732

733 Alvarez L, Dai L, Friedrich BM, Kashikar ND, Gregor I, Pascal R, *et al.* 2012. The rate of change in Ca<sup>2+</sup>  
734 concentration controls sperm chemotaxis. *J. Cell Biol.* **196**:653-663. 10.1083/jcb.201106096

735

736 Billard R. 1986. Spermatogenesis and spermatology of some teleost fish species. *Reprod. Nutr. Dev.* **26**:877-920.

737

738 Böhmer M, Van Q, Weyand I, Hagen V, Beyermann M, Matsumoto M, *et al.* 2005. Ca<sup>2+</sup> spikes in the flagellum  
739 control chemotactic behavior of sperm. *EMBO J.* **24**:2741-2752.

740

741 Bönigk W, Loogen A, Seifert R, Kashikar N, Klemm C, Krause E, *et al.* 2009. An atypical CNG channel  
742 activated by a single cGMP molecule controls sperm chemotaxis. *Sci. Signal.* **2**:ra68.

743

744 Boron WF De Weer P. 1976. Intracellular pH transients in squid giant axons caused by CO<sub>2</sub>, NH<sub>3</sub>, and  
745 metabolic inhibitors. *J. Gen. Physiol.* **67**:91-112.

746

747 Brams M, Kusch J, Spurny R, Benndorf K Ulens C. 2014. Family of prokaryote cyclic nucleotide-modulated ion  
748 channels. *Proc. Natl. Acad. Sci. USA* **111**:7855-7860. 10.1073/pnas.1401917111

749

750 Brelidze TI, Carlson AE, Davies DR, Stewart LJ Zagotta WN. 2010. Identifying regulators for EAG1 channels  
751 with a novel electrophysiology and tryptophan fluorescence based screen. *PLoS one* **5**  
752 10.1371/journal.pone.0012523

753

754 Brelidze TI, Carlson AE, Sankaran B Zagotta WN. 2012. Structure of the carboxy-terminal region of a KCNH  
755 channel. *Nature* **481**:530-533. 10.1038/nature10735

756

757 Brelidze TI, Carlson AE Zagotta WN. 2009. Absence of direct cyclic nucleotide modulation of mEAG1 and  
758 hERG1 channels revealed with fluorescence and electrophysiological methods. *J. Biol. Chem.*

759

760 Brenker C, Goodwin N, Weyand I, Kashikar ND, Naruse M, Krähling M, *et al.* 2012. The CatSper channel: a  
761 polymodal chemosensor in human sperm. *EMBO J.* **31**:1654-1665.

762  
763 Brenker C, Zhou Y, Müller A, Echeverry FA, Trötschel C, Poetsch A, *et al.* 2014. The Ca<sup>2+</sup>-activated K<sup>+</sup> current  
764 of human sperm is mediated by Slo3. *eLife* **3**:e01438. 10.7554/eLife.01438

765  
766 Carlson AE, Brelidze TI Zagotta WN. 2013. Flavonoid regulation of EAG1 channels. *J. Gen. Physiol.* **141**:347-  
767 358. 10.1085/jgp.201210900

768  
769 Chavez JC, de la Vega-Beltran JL, Escoffier J, Visconti PE, Trevino CL, Darszon A, *et al.* 2013. Ion  
770 permeabilities in mouse sperm reveal an external trigger for SLO3-dependent hyperpolarization. *PLoS one*  
771 **8**:e60578. 10.1371/journal.pone.0060578

772  
773 Cherr GN, Morisawa M, Vines CA, Yoshida K, Smith EH, Matsubara T, *et al.* 2008. Two egg-derived molecules  
774 in sperm motility initiation and fertilization in the Pacific herring (*Clupea pallasii*). *Int. J. Dev. Biol.* **52**:743-752.

775  
776 Chung JJ, Shim SH, Everley RA, Gygi SP, Zhuang X Clapham DE. 2014. Structurally distinct Ca<sup>2+</sup> signaling  
777 domains of sperm flagella orchestrate tyrosine phosphorylation and motility. *Cell* **157**:808-822.  
778 10.1016/j.cell.2014.02.056

779  
780 Clayton GM, Silverman WR, Heginbotham L Morais-Cabral JH. 2004. Structural basis of ligand activation in a  
781 cyclic nucleotide regulated potassium channel. *Cell* **119**:615-627.

782  
783 Cosson J, Groison AL, Suquet M, Fauvel C, Dreanno C Billard R. 2008. Marine fish spermatozoa: racing  
784 ephemeral swimmers. *Reproduction* **136**:277-294. 10.1530/REP-07-0522

785  
786 Cukkemane A, Grüter B, Novak K, Gensch T, Bönigk W, Gerharz T, *et al.* 2007. Subunits act independently in a  
787 cyclic nucleotide-activated K<sup>+</sup> channel. *EMBO Reports* **8**:749-755.

788  
789 Darszon A, Acevedo JJ, Galindo BE, Hernández-González EO, Nishigaki T, Treniño CL, *et al.* 2006. Sperm  
790 channel diversity and functional multiplicity. *Reproduction* **131**:977-988.

791  
792 Darszon A, Guerrero A, Galindo BE, Nishigaki T Wood CD. 2008. Sperm-activating peptides in the regulation  
793 of ion fluxes, signal transduction and motility. *Int. J. Dev. Biol.* **52**:595-606.

794  
795 Denissenko P, Kantsler V, Smith DJ Kirkman-Brown J. 2012. Human spermatozoa migration in microchannels  
796 reveals boundary-following navigation. *Proc. Natl. Acad. Sci. USA* **109**:8007-8010. 10.1073/pnas.1202934109

797  
798 Dhallan RS, Yau K-W, Schrader KA Reed RR. 1990. Primary structure and functional expression of a cyclic  
799 nucleotide-activated channel from olfactory neurons. *Nature* **347**:184-187.

800  
801 Dorfer V, Pichler P, Stranzl T, Stadlmann J, Taus T, Winkler S, *et al.* 2014. MS Amanda, a universal  
802 identification algorithm optimized for high accuracy tandem mass spectra. *J. Proteome Res.* **13**:3679-3684.  
803 10.1021/pr500202e

804  
805 Dziewulska K Domagala J. 2013. Effect of pH and cation concentrations on spermatozoan motility of sea trout  
806 (*Salmo trutta m. trutta* L.). *Theriogenology* **79**:48-58. 10.1016/j.theriogenology.2012.09.008

807

808 Eisenbach M Giojalas LC. 2006. Sperm guidance in mammals - an unpaved road to the egg. *Nat. Rev. Mol. Cell*  
809 *Biol.* **7**:276-285.

810  
811 Elgeti J, Kaupp UB Gompper G. 2010. Hydrodynamics of sperm cells near surfaces. *Biophys. J.* **99**:1018-1026.

812  
813 Fakler B, Brandle U, Glowatzki E, Weidemann S, Zenner HP Ruppertsberg JP. 1995. Strong voltage-dependent  
814 inward rectification of inward rectifier K<sup>+</sup> channels is caused by intracellular spermine. *Cell* **80**:149-154.

815  
816 Florman HM, Jungnickel MK Sutton KA. 2008. Regulating the acrosome reaction. *Int. J. Dev. Biol.* **52**:503-510.

817  
818 Gakamsky A, Armon L Eisenbach M. 2009. Behavioral response of human spermatozoa to a concentration jump  
819 of chemoattractants or intracellular cyclic nucleotides. *Hum. Reprod.* **24**:1152-1163. 10.1093/humrep/den409

820  
821 Gauss R, Seifert R Kaupp UB. 1998. Molecular identification of a hyperpolarization-activated channel in sea  
822 urchin sperm. *Nature* **393**:583-587.

823  
824 Guerrero A, Wood CD, Nishigaki T, Carneiro J Darszon A. 2010. Tuning sperm chemotaxis.  
825 *Biochem.Soc.Trans.* **38**:1270-1274.

826  
827 Hagen V, Frings S, Wiesner B, Helm S, Kaupp UB Bendig J. 2003. [7-(Dialkylamino)coumarin-4-yl]methyl-  
828 caged compounds as ultrafast and effective long-wavelength phototriggers of 8-bromo-substituted cyclic  
829 nucleotides. *Chem. Bio. Chem.* **4**:434-442.

830  
831 Hart NH Danovan M. 1983. Fine-structure of the chorion and site of sperm entry in the egg of Brachydanio. *J.*  
832 *Exp. Zool.* **227**:277-296.

833  
834 Hirohashi N, Alvarez L, Shiba K, Fujiwara E, Iwata Y, Mohri T, *et al.* 2013. Sperm from sneaker male squids  
835 exhibit chemotactic swarming to CO<sub>2</sub>. *Curr. Biol.* **23**:775-781. 10.1016/j.cub.2013.03.040

836  
837 Ho H-C Suarez SS. 2001. Hyperactivation of mammalian spermatozoa: function and regulation. *Reproduction*  
838 **122**:519-526.

839  
840 Hugentobler SA, Morris DG, Sreenan JM Diskin MG. 2007. Ion concentrations in oviduct and uterine fluid and  
841 blood serum during the estrous cycle in the bovine. *Theriogenology* **68**:538-548.  
842 10.1016/j.theriogenology.2007.04.049

843  
844 Iwamatsu T, Yoshizaki N Shibata Y. 1997. Changes in the chorion and sperm entry into the micropyle during  
845 fertilization in the teleostean fish, *Oryzias latipes*. *Dev. Growth Differ.* **39**:33-41.

846  
847 Käll L, Canterbury JD, Weston J, Noble WS MacCoss MJ. 2007. Semi-supervised learning for peptide  
848 identification from shotgun proteomics datasets. *Nat. Methods* **4**:923-925. 10.1038/nmeth1113

849  
850 Kashikar ND, Alvarez L, Seifert R, Gregor I, Jäckle O, Beyermann M, *et al.* 2012. Temporal sampling, resetting,  
851 and adaptation orchestrate gradient sensing in sperm. *J. Cell Biol.* **198**:1075-1091.

852  
853 Kaupp UB, Kashikar ND Weyand I. 2008. Mechanisms of sperm chemotaxis. *Annu. Rev. Physiol.* **70**:93-117.

854  
855 Kaupp UB Seifert R. 2002. Cyclic nucleotide-gated ion channels. *Physiol. Rev.* **82**:769-824.

856  
857 Kaupp UB, Solzin J, Hildebrand E, Brown JE, Helbig A, Hagen V, *et al.* 2003. The signal flow and motor  
858 response controlling chemotaxis of sea urchin sperm. *Nat. Cell Biol.* **5**:109-117.

859  
860 Kesters D, Brams M, Nys M, Wijckmans E, Spurny R, Voets T, *et al.* 2015. Structure of the SthK carboxy-  
861 terminal region reveals a gating mechanism for cyclic nucleotide-modulated ion channels. *PLoS one*  
862 **10**:e0116369. 10.1371/journal.pone.0116369

863  
864 Kim C, Cheng CY, Saldanha SA Taylor SS. 2007. PKA-I holoenzyme structure reveals a mechanism for cAMP-  
865 dependent activation. *Cell* **130**:1032-1043. 10.1016/j.cell.2007.07.018

866  
867 Kirichok Y, Navarro B Clapham DE. 2006. Whole-cell patch-clamp measurements of spermatozoa reveal an  
868 alkaline-activated Ca<sup>2+</sup> channel. *Nature* **439**:737-740.

869  
870 Körschen HG, Beyermann M, Müller F, Heck M, Vantler M, Koch K-W, *et al.* 1999. Interaction of glutamic-  
871 acid-rich proteins with the cGMP signalling pathway in rod photoreceptors. *Nature* **400**:761-766.

872  
873 Körschen HG, Illing M, Seifert R, Sesti F, Williams A, Gotzes S, *et al.* 1995. A 240 kDa protein represents the  
874 complete  $\beta$  subunit of the cyclic nucleotide-gated channel from rod photoreceptor. *Neuron* **15**:627-636.

875  
876 Krasznai Z, Márián T, Izumi H, Damjanovich S, Balkay L, Trón L, *et al.* 2000. Membrane hyperpolarization  
877 removes inactivation of Ca<sup>2+</sup> channels, leading to Ca<sup>2+</sup> influx and subsequent initiation of sperm motility in the  
878 common carp. *Proc. Natl. Acad. Sci. USA* **97**:2052-2057.

879  
880 Lee HC. 1984. Sodium and proton transport in flagella isolated from sea urchin spermatozoa. *J. Biol. Chem.*  
881 **259**:4957-4963.

882  
883 Lee HC. 1985. The voltage-sensitive Na<sup>+</sup>/H<sup>+</sup> exchange in sea urchin spermatozoa flagellar membrane vesicles  
884 studied with an entrapped pH probe. *J. Biol. Chem.* **260**:10794-10799.

885  
886 Lee HC Garbers DL. 1986. Modulation of the voltage-sensitive Na<sup>+</sup>/H<sup>+</sup> exchange in sea urchin spermatozoa  
887 through membrane potential changes induced by the egg peptide speract. *J. Biol. Chem.* **261**:16026-16032.

888  
889 Levin TC King N. 2013. Evidence for sex and recombination in the choanoflagellate *Salpingoeca rosetta*. *Curr.*  
890 *Biol.* **23**:2176-2180. 10.1016/j.cub.2013.08.061

891  
892 Liman ER, Tytgat J Hess P. 1992. Subunit stoichiometry of a mammalian K<sup>+</sup> channel determined by  
893 construction of multimeric cDNAs. *Neuron* **9**:861-871.

894  
895 Lishko PV, Botchkina IL, Fedorenko A Kirichok Y. 2010. Acid extrusion from human spermatozoa is mediated  
896 by flagellar voltage-gated proton channel. *Cell* **140**:327-337.

897  
898 Lishko PV, Botchkina IL Kirichok Y. 2011. Progesterone activates the principal Ca<sup>2+</sup> channel of human sperm.  
899 *Nature* **471**:387-391.

900  
901 Lishko PV Kirichok Y. 2010. The role of Hv1 and CatSper channels in sperm activation. *J. Physiol.* **588**:4667-  
902 4672. 10.1113/jphysiol.2010.194142

903

904 Lishko PV, Kirichok Y, Ren D, Navarro B, Chung JJ Clapham DE. 2012. The control of male fertility by  
905 spermatozoan ion channels. *Annu. Rev. Physiol.* **74**:453-475. 10.1146/annurev-physiol-020911-153258

906  
907 Matsuda H, Saigusa A, Irisawa H. 1987. Ohmic conductance through the inwardly rectifying K channel and  
908 blocking by internal  $Mg^{2+}$ . *Nature* **325**:156-159.

909  
910 Morisawa M. 2008. Adaptation and strategy for fertilization in the sperm of teleost fish. *J. Appl. Ichthyol.*  
911 **24**:362-370.

912  
913 Morisawa M, Suzuki K, Shimizu H, Morisawa S, Yasuda K. 1983. Effects of osmolality and potassium on  
914 motility of spermatozoa from freshwater cyprinid fishes. *J. Exp. Biol.* **107**:95-103.

915  
916 Navarro B, Kirichok Y, Clapham DE. 2007. KSper, a pH-sensitive  $K^+$  current that controls sperm membrane  
917 potential. *Proc. Natl. Acad. Sci. USA* **104**:7688-7692.

918  
919 Nishigaki T, Jose O, Gonzalez-Cota AL, Romero F, Trevino CL, Darszon A. 2014. Intracellular pH in sperm  
920 physiology. *Biochem. Biophys. Res. Commun.* **450**:1149-1158. 10.1016/j.bbrc.2014.05.100

921  
922 Nobrega RH, Batlouni SR, Franca LR. 2009. An overview of functional and stereological evaluation of  
923 spermatogenesis and germ cell transplantation in fish. *Fish. Physiol. Biochem.* **35**:197-206. 10.1007/s10695-008-  
924 9252-z

925  
926 Ohta T, Iwamatsu T. 1983. Electron microscopic observations on sperm entry into eggs of the rose bitterling,  
927 *Rhodeus ocellatus*. *J. Exp. Zool.* **227**:109-119. 10.1002/jez.1402270115

928  
929 Page RD. 1996. TreeView: an application to display phylogenetic trees on personal computers. *Comput. Appl.*  
930 *Biosci.* **12**:357-358.

931  
932 Pichlo M, Bungert-Plümke S, Weyand I, Seifert R, Bönigk W, Strünker T, *et al.* 2014. High density and ligand  
933 affinity confer ultrasensitive signal detection by a guanylyl cyclase chemoreceptor. *J. Cell Biol.* **206**:541-557.  
934 10.1083/jcb.201402027

935  
936 Publicover SJ, Giojalas LC, Teves ME, de Oliveira GS, Garcia AA, Barratt CL, *et al.* 2008.  $Ca^{2+}$  signalling in  
937 the control of motility and guidance in mammalian sperm. *Front Biosci.* **13**:5623-5637.

938  
939 Rehmann H, Prakash B, Wolf E, Rueppel A, de Rooij J, Bos JL, *et al.* 2003. Structure and regulation of the  
940 cAMP-binding domains of Epac2. *Nat. Struct. Biol.* **10**:26-32.

941  
942 Santi CM, Butler A, Kuhn J, Wei A, Salkoff L. 2009. Bovine and mouse SLO3  $K^+$  channels: evolutionary  
943 divergence points to an RCK1 region of critical function. *J. Biol. Chem.* **284**:21589-21598.  
944 10.1074/jbc.M109.015040

945  
946 Santi CM, Santos T, Hernández-Cruz A, Darszon A. 1998. Properties of a novel pH-dependent  $Ca^{2+}$  permeation  
947 pathway present in male germ cells with possible roles in spermatogenesis and mature sperm function. *J. Gen.*  
948 *Physiol.* **112**:33-53.

949  
950 Schreiber M, Wei A, Yuan A, Gaut J, Saito M, Salkoff L. 1998. Slo3, a novel pH-sensitive  $K^+$  channel from  
951 mammalian spermatocytes. *J. Biol. Chem.* **273**:3509-3516.

952

953 Schünke S, Stoldt M, Lecher J, Kaupp UB Willbold D. 2011. Structural insights into conformational changes of  
954 a cyclic nucleotide-binding domain in solution from *Mesorhizobium loti* K1 channel. *Proc. Natl. Acad. Sci. USA*  
955 **108**:6121-6126.

956  
957 Schünke S, Stoldt M, Novak K, Kaupp UB Willbold D. 2009. Solution structure of the *Mesorhizobium loti* K1  
958 channel cyclic nucleotide-binding domain in complex with cAMP. *EMBO Rep.* **10**:729-735.

959  
960 Seifert R, Flick M, Bönigk W, Alvarez L, Trötschel C, Poetsch A, *et al.* 2015. The CatSper channel controls  
961 chemosensation in sea urchin sperm. *EMBO J.* **34**:379-392.

962  
963 Selman K, Wallace RA, Sarka A Qi X. 1993. Stages of Oocyte Development in the Zebrafish, *Brachydanio*  
964 *rerio*. *J. Morph.* **218**:203-224.

965  
966 Smith JF, Syritysyna O, Fellous M, Serres C, Mannowetz N, Kirichok Y, *et al.* 2013. Disruption of the principal,  
967 progesterone-activated sperm Ca<sup>2+</sup> channel in a CatSper2-deficient infertile patient. *Proc. Natl. Acad. Sci. USA*  
968 **110**:6823-6828.

969  
970 Stein I, Itin A, Einat P, Skaliter R, Grossman Z Keshet E. 1998. Translation of vascular endothelial growth factor  
971 mRNA by internal ribosome entry: implications for translation under hypoxia. *Mol. Cell. Biol.* **18**:3112-3119.

972  
973 Strünker T, Goodwin N, Brenker C, Kashikar ND, Weyand I, Seifert R, *et al.* 2011. The CatSper channel  
974 mediates progesterone-induced Ca<sup>2+</sup> influx in human sperm. *Nature* **471**:382-386.

975  
976 Strünker T, Weyand I, Bönigk W, Van Q, Loogen A, Brown JE, *et al.* 2006. A K<sup>+</sup>-selective cGMP-gated ion  
977 channel controls chemosensation of sperm. *Nat. Cell Biol.* **8**:1149-1154.

978  
979 Takai H Morisawa M. 1995. Change in intracellular K<sup>+</sup> concentration caused by external osmolality change  
980 regulates sperm motility of marine and freshwater teleosts. *J. Cell Sci.* **108**:1175-1181.

981  
982 Umen J Heitman J. 2013. Evolution of sex: mating rituals of a pre-metazoan. *Curr. Biol.* **23**:R1006-1008.  
983 10.1016/j.cub.2013.10.009

984  
985 Vines CA, Yoshida K, Griffin FJ, Pillai MC, Morisawa M, Yanagimachi R, *et al.* 2002. Motility initiation in  
986 herring sperm is regulated by reverse sodium-calcium exchange. *Proc. Natl. Acad. Sci. USA* **99**:2026-2031.

987  
988 Wilson-Leedy JG, Kanuga MK Ingermann RL. 2009. Influence of osmolality and ions on the activation and  
989 characteristics of zebrafish sperm motility. *Theriogenology* **71**:1054-1062.  
990 10.1016/j.theriogenology.2008.11.006

991  
992 Wood CD, Nishigaki T, Furuta T, Baba SA Darszon A. 2005. Real-time analysis of the role of Ca<sup>2+</sup> in flagellar  
993 movement and motility in single sea urchin sperm. *J. Cell Biol.* **169**:725-731.

994  
995 Yanagimachi R, Cherr G, Matsubara T, Andoh T, Harumi T, Vines C, *et al.* 2013. Sperm attractant in the  
996 micropyle region of fish and insect eggs. *Biol. Reprod.* **88**:47. 10.1095/biolreprod.112.105072

997  
998 Yanagimachi R, Cherr GN, Pillai MC Baldwin JD. 1992. Factors controlling sperm entry into the micropyles of  
999 salmonid and herring eggs. *Dev. Growth Differ.* **34**:447-461.

1000

1001 Yang C, Zeng XH, Zhou Y, Xia XM Lingle CJ. 2011. LRRC52 (leucine-rich-repeat-containing protein 52), a  
1002 testis-specific auxiliary subunit of the alkalization-activated Slo3 channel. *Proc. Natl. Acad. Sci. USA*  
1003 **108**:19419-19424.

1004  
1005 Yoshida M Yoshida K. 2011. Sperm chemotaxis and regulation of flagellar movement by Ca<sup>2+</sup>. *Mol. Hum.*  
1006 *Reprod.* **17**:457-465. 10.1093/molehr/gar041

1007  
1008 Zagotta WN, Olivier NB, Black KD, Young EC, Olson R Gouaux E. 2003. Structural basis for modulation and  
1009 agonist specificity of HCN pacemaker channels. *Nature* **425**:200-205.

1010  
1011 Zeng XH, Navarro B, Xia XM, Clapham DE Lingle CJ. 2013. Simultaneous knockout of Slo3 and CatSper1  
1012 abolishes all alkalization- and voltage-activated current in mouse spermatozoa. *J. Gen. Physiol.* **142**:305-313.  
1013 10.1085/jgp.201311011

1014  
1015 Zeng XH, Yang C, Kim ST, Lingle CJ Xia XM. 2011. Deletion of the Slo3 gene abolishes alkalization-activated  
1016 K<sup>+</sup> current in mouse spermatozoa. *Proc. Natl. Acad. Sci. USA* **108**:5879-5884.

1017  
1018 Zhang X, Zeng X Lingle CJ. 2006a. Slo3 K<sup>+</sup> channels: voltage and pH dependence of macroscopic currents. *J.*  
1019 *Gen. Physiol.* **128**:317-336.

1020  
1021 Zhang X, Zeng X, Xia XM Lingle CJ. 2006b. pH-regulated Slo3 K<sup>+</sup> channels: properties of unitary currents. *J.*  
1022 *Gen. Physiol.* **128**:301-315. 10.1085/jgp.200609551

1023  
1024  
1025

1026 **Figure Legends**

1027

1028 **Figure 1. Identification of *Dr*CNGK channel homologues and of a K<sup>+</sup> channel in *D. rerio***  
1029 **sperm.**

1030 (A) Phylogenetic tree (Page, 1996) of various ion channel families. The CNGK channel  
1031 family exists in protozoa (dark blue), marine invertebrates and fish (medium blue), and  
1032 freshwater fish (light blue). The HCN, CNG, and KCNH channel families are highlighted in  
1033 green; voltage-gated Na<sub>v</sub> and Ca<sub>v</sub> channels are highlighted in yellow; and voltage-gated K<sub>v</sub>  
1034 channels are highlighted in red. The following ion channel sequences were used: CNGK  
1035 channels from zebrafish (*Dr*CNGK), rainbow trout (*Om*CNGK), spotted gar (*Lo*CNGK),  
1036 West Indian Ocean coelacanth (*Lc*CNGK), sea urchin (*Ap*CNGK), acorn worm (*Sk*CNGK),  
1037 amphioxus (*Bf*CNGK), starlet sea anemone (*Nv*CNGK), vasa tunicate (*Ci*CNGK), sponge  
1038 (*Aq*CNGK), choanoflagellate (*Sr*CNGK); murine HCN channel subunits 1 (*m*HCN1), 2  
1039 (*m*HCN2), 3 (*m*HCN3), 4 (*m*HCN4), and the HCN channel from sea urchin (*Sp*HCN1); rat  
1040 CNGA subunits A1 (*r*CNGA1), A2 (*r*CNGA2), A3 (*r*CNGA3), and A4 (*r*CNGA4); the  
1041 KCNH channels from fruit fly (*Dm*EAG) and human (hERG); murine voltage-gated Na<sub>v</sub>  
1042 (*m*Na<sub>v</sub> 1.1 and *m*Na<sub>v</sub> 1.6) and Ca<sub>v</sub> channels (*m*Ca<sub>v</sub>1.1, *m*Ca<sub>v</sub>2.3 and *m*Ca<sub>v</sub>3.1) and voltage-  
1043 gated K<sub>v</sub> channels from fruit fly (*Dm*Shaker) and mouse (*m*K<sub>v</sub>3.1). Full-length Latin names  
1044 and accession numbers are given in experimental procedures. Scale bar represents 0.1  
1045 substitutions per site. (B) Pseudo-tetrameric structure of CNGK channels. Numbers 1 to 4,  
1046 homologous repeats; S1 to S6, transmembrane segments; yellow cylinders, cyclic nucleotide-  
1047 binding domain CNBD; asterisks, epitopes recognized by antibodies anti-repeat1 of *Dr*CNGK  
1048 (polyclonal) and anti-repeat3 of *Dr*CNGK (YENT1E2, monoclonal). (C) Whole-cell  
1049 recordings from zebrafish sperm at low (left upper panel) and high (middle panel)  
1050 extracellular K<sup>+</sup> concentrations. Left lower panel: Voltage step protocol. Right panel:  
1051 corresponding IV relations. (D) Whole-cell recordings from an isolated sperm head.

1052 Description see part C. (E) Whole-cell recording from zebrafish sperm (upper panel) and an  
1053 isolated head (lower panel). (F) IV relation of recordings from part E. (G) Pooled IV relations  
1054 ( $\pm$  sd) of currents from zebrafish sperm (filled circle,  $n = 23$ ) and sperm heads (open squares,  
1055  $n = 6$ ).

1056

1057 **Figure 2. Localization of the DrCNGK channel.**

1058 (A) Western blot of membrane proteins (15  $\mu$ g) from CHOK1 cells transfected with cDNA  
1059 encoding either *DrCNGK* with a C-terminal HA-tag alone (lane C) or with both, a C-terminal  
1060 HA-tag and an N-terminal flag-tag (N/C). Apparent molecular weight  $M_w$  is indicated on the  
1061 left. (B) Characterization of anti-*DrCNGK* antibodies. Left: Western blot of membrane  
1062 proteins (10  $\mu$ g) from HEK293 cells transfected with cDNA encoding *DrCNGK* (Tr) and  
1063 wild-type cells (wt). Right: Western blot of membrane proteins (15  $\mu$ g) from zebrafish testis.  
1064 (C) Western blot of membrane proteins (15  $\mu$ g) from different zebrafish tissues. (D) Upper  
1065 panel: Scheme of a testis cross-section. GC, germinal compartment; IC, intertubular  
1066 compartment; SER, Sertoli cells; SGA, primary spermatogonia; SGB, secondary  
1067 spermatogonia; SC, spermatocytes; ST, spermatids scheme according to (Nobrega et al.,  
1068 2009). Lower panel: Staining with anti-repeat1 antibody (red, left) and superposition (right) of  
1069 the immunohistochemical image with a bright-field image of an *in situ* hybridization using an  
1070 anti-*DrCNGK*-specific RNA probe (arrows). Bar represents 50  $\mu$ m. (E) Staining of zebrafish  
1071 sperm with anti-repeat1 (upper left panel) and anti-repeat3 antibody (lower left panel). Bars  
1072 represent 10  $\mu$ m. The respective bright-field images are shown (upper and lower right panels).  
1073 (F) Western blot of equal amounts of total membrane proteins (15  $\mu$ g) from purified heads  
1074 and purified flagella.

1075

1076 **Figure 3. Cyclic nucleotides do not activate K<sup>+</sup> channels in sperm.**

1077 (A) Current amplitude of whole-cell recordings from zebrafish sperm at +25 mV in the  
1078 absence or presence of 100  $\mu$ M cAMP or cGMP in the pipette (control:  $91 \pm 49$  pA ( $n = 23$ );  
1079 cAMP:  $73 \pm 25$  pA ( $n = 6$ ); cGMP:  $109 \pm 44$  pA ( $n = 5$ )). Individual data (symbols) and mean  
1080  $\pm$  sd (gray bars), number of experiments in parentheses. (B) Photo-release of cyclic  
1081 nucleotides from caged precursors inside sperm. Left panel: Whole-cell recordings at +15 mV  
1082 from sperm loaded with 100  $\mu$ M BCMACM-caged cAMP (upper panel) or BCMACM-caged  
1083 cGMP (lower panel). Arrows indicate the delivery of the UV flash to release cyclic  
1084 nucleotides by photolysis. Right panel: Mean current 3 s before (-) and 3 s after (+) the release  
1085 of cAMP or cGMP. Statistics as in part A. Data points from individual sperm are indicated by  
1086 identical colours. (C-F) Currents of heterologously expressed *DrCNGK* channels in the  
1087 absence or presence of 8-Bromo analogs of cyclic nucleotides. (C) Left: Two-Electrode  
1088 Voltage-Clamp recordings from *DrCNGK*-injected *Xenopus* oocytes. Currents shown are in  
1089 the absence (left traces) and presence (right traces) of 10 mM 8Br-cAMP. Voltage steps as  
1090 shown in Figure 3-figure supplement 1A. Right: relations of current recordings from the left  
1091 panel. (D) Pooled IV curves from *DrCNGK* injected and control oocytes; recordings in the  
1092 absence and presence of 10 mM 8Br-cAMP. (E) Left: Two-Electrode Voltage-Clamp  
1093 recordings from *DrCNGK* injected *Xenopus* oocytes. Currents shown are in the absence (left  
1094 traces) and presence (right traces) of 10 mM 8Br-cGMP. (F) Pooled IV curves I from  
1095 *DrCNGK*-injected and control oocytes; recordings in the absence and presence of 10 mM  
1096 8Br-cGMP. (G) Swimming path before (green line) and after (red line) photo-release (black  
1097 flash) of cAMP (left panel) or cGMP (right panel). The blue arrow indicates the swimming  
1098 direction. Photo-release of cyclic nucleotides was verified by monitoring the increase of  
1099 fluorescence of the caging group (Figure 3-figure supplement 5) (Hagen et al., 2003). (H)  
1100 Path curvature before (-) and after (+) release of cAMP or cGMP. Sperm were loaded with 30  
1101  $\mu$ M DEACM-caged cAMP or DEACM-caged cGMP. Statistics as in part A.

1102 **Figure 4. Comparison of sperm K<sup>+</sup> current with current from heterologously expressed**  
1103 ***ApCNGK* channels.**

1104 (A) Normalized IV relations of whole-cell recordings from zebrafish sperm and *ApCNGK*  
1105 channels expressed in HEK293 cells. Pipette solution: standard IS. Bath solution: standard  
1106 ES. Currents were normalized to -1 at -115 mV. (B) Normalized IV relations (mean current ±  
1107 sd, n = 6) of inside-out recordings from *ApCNGK* channels expressed in HEK293 cells.  
1108 Pipette solution: standard ES, bath solution: NMDG-based IS with the indicated  
1109 concentrations of Na<sup>+</sup>, Mg<sup>2+</sup>, and spermine. Currents were normalized to -1 at -103 mV. (C)  
1110 Alignment of pore regions from different CNGK channels. Freshwater fishes are highlighted  
1111 in light blue and seawater species in dark blue. The position of the last amino-acid residue is  
1112 given on the right. Asterisks indicate the G(Y/F)GD selectivity motif. A key threonine residue  
1113 that is conserved in three repeats of the *ApCNGK* channel and other seawater species is  
1114 highlighted in red (arrow). Hydrophobic amino acids at this position are indicated in gray. (D)  
1115 IV relations of inside-out recordings of *ApCNGK* channels expressed in HEK293 cells.  
1116 Pipette solution: ES; bath solution: NMDG-based IS. Different Na<sup>+</sup> concentrations were  
1117 added to the bath solution. (E) Normalized IV relations (mean current ± sd) of whole-cell  
1118 recordings from zebrafish sperm (n = 18) and from *ApCNGK-4V* channels (n = 7) expressed  
1119 in HEK293 cells. Currents were normalized to -1 at -115 mV. Inset: amino-acid sequence of  
1120 the pore region of the mutant *ApCNGK-4V*. *ApCNGK* channels were activated with 100 μM  
1121 cGMP.

1122

1123 **Figure 5. pH regulation of the *DrCNGK* channel.**

1124 (A) Whole-cell recordings from zebrafish sperm after perfusion with NH<sub>4</sub>Cl or propionic acid.  
1125 Voltage steps as shown in Figure 1C. Recordings at extracellular pH 7.4 and pipette pH 6.4

1126 (left).  $\text{NH}_4\text{Cl}$  (10 mM, middle) or propionic acid (10 mM, right) was added to the bath. (B)  
1127 Pooled IV curves for recordings from zebrafish sperm at a pipette  $\text{pH}_i$  of 6.4 and in the  
1128 presence of 10 mM  $\text{NH}_4\text{Cl}$  or 10 mM propionic acid (PA). (C) Pooled IV curves from  
1129 recordings of zebrafish sperm at different intracellular  $\text{pH}_i$ . (D) Dependence of mean current  
1130 ( $\pm$  sd) on intracellular  $\text{pH}_i$  (circles, bottom axis) or in the presence of either 10 mM propionic  
1131 acid (PA) or different  $\text{NH}_4\text{Cl}$  concentrations (triangles, top axis). (E) Recording of the voltage  
1132 signal of zebrafish sperm in the current-clamp configuration. Pipette solution with an  
1133 intracellular  $\text{pH}_i$  of 6.4; recording in the presence of 10 mM  $\text{NH}_4\text{Cl}$  or 10 mM propionic acid  
1134 (PA). Left panel: single recording. Right panel: individual data (symbols) and mean  $\pm$  sd  
1135 (gray bars),  $n = 10$ . (F) Pooled IV curves of Two-Electrode Voltage-Clamp recordings from  
1136 heterologously expressed *DrCNGK* channels and uninjected wild-type oocytes in 96 mM  $\text{K}^+$   
1137 bicarbonate solution (black and red symbols) or 96 mM  $\text{K}^+$  gluconate, including 1 mM  $\text{NH}_4\text{Cl}$   
1138 (white symbols, see Figure 5-figure supplement 1 for recordings). (G) Changes in  
1139 fluorescence of a zebrafish sperm population incubated with the pH indicator BCECF,  
1140 recorded as the ratio of fluorescence at 549/15 nm and 494/20 nm (excited at 452/28 nm),  
1141 before (black) and after the addition of 10 mM (red) or 30 mM (green)  $\text{NH}_4\text{Cl}$ . (H)  
1142 Stimulation of sperm with  $\text{NH}_4\text{Cl}$  as in panel G using the  $\text{Ca}^{2+}$  indicator Cal-520.  
1143 Fluorescence was excited at 494/20 nm and recorded at 536/40 nm. Fluorescence F was  
1144 normalized to the control value  $F_0$  before stimulation.

1145

1146 **Figure 6. Sperm swimming behaviour upon  $\text{Ca}^{2+}$  release.**

1147 (A), (B), and (C) representative swimming paths of three different DMSO loaded sperm  
1148 before and after application of UV light. (D), (E), and (F) representative averaged swimming  
1149 paths of three different sperm before (green) and after  $\text{Ca}^{2+}$  release by one (red) or two (cyan)  
1150 consecutive UV flashes (black arrows). Curved blue arrows indicate the swimming direction

1151 of sperm. (G) Same swimming path shown in (F) including a temporal axis to facilitate the  
1152 visualization of the changes in swimming path after consecutive flashes. Upon release (black  
1153 arrows), the curvature of the swimming path progressively increases and the cell finally spins  
1154 around the same position. (H) Representative flagellar shapes before (-), after  $\text{Ca}^{2+}$  release by  
1155 one (+) or two consecutive flashes (++), and during cell spinning against the wall (bottom  
1156 right). Consecutive frames every 100 ms are shown in different colours. Sequence order: red,  
1157 green, blue, and yellow. (I) Mean curvature before (-) and after one (+) or two (++) UV  
1158 flashes. Individual data (symbols) and mean  $\pm$  sd (gray bars), number of experiments in  
1159 parentheses.

1160

1161 **Figure 7. Models of signalling pathways in sea urchin and zebrafish sperm.**

1162 Sea urchin (upper panel): Binding of the chemoattractant resact to a receptor guanylyl cyclase  
1163 (GC) activates cGMP synthesis. Cyclic GMP opens  $\text{K}^+$ -selective CNG channels (CNGK),  
1164 thereby, causing a hyperpolarization, which in turn activates a sperm-specific  $\text{Na}^+/\text{H}^+$   
1165 exchanger (sNHE) that alkalizes the cell. Alkalization and subsequent depolarization by  
1166 hyperpolarization-activated and cyclic nucleotide-gated (HCN) channels lead to the opening  
1167 of sperm-specific CatSper channels. Zebrafish (lower panel): Upon spawning,  $\text{K}^+$  efflux  
1168 through CNGK hyperpolarizes sperm. An unknown mechanism of alkalization (dashed lines)  
1169 modulates the open probability of CNGK channels; the ensuing hyperpolarization opens  
1170 voltage-gated  $\text{Ca}^{2+}$  channels ( $\text{Ca}_v$ ).

1171 **Video 1. Behavioural response of zebrafish sperm to successive  $\text{Ca}^{2+}$  release**

1172 Representative recording of zebrafish sperm loaded with NP-EGTA (40  $\mu\text{M}$ ). Upon release of  
1173  $\text{Ca}^{2+}$ , the swimming path curvature increases and, eventually, sperm spin against the wall of  
1174 the recording chamber with their flagellum pointing away from the wall. Video recorded

1175 using dark-field microscopy at 30 frames per second using a 20x magnification objective. The  
1176 field of view corresponds to 410  $\mu\text{m}$ . The Video is shown in real time.

1177

1178 **Supporting Information**

1179

1180 **Figure 1-figure supplement 1. Amino-acid sequence of the *Dr*CNGK channel**

1181 Different colors indicate the transmembrane segments (red shades, repeats 1-4), the four pore  
1182 regions (green), the four CNBDs (gray), and the unusual insert in the C-linker of the third  
1183 repeat (blue). Lines below the sequence indicate peptides that were identified by mass  
1184 spectrometry in testis and sperm preparations. The position of the last amino-acid residue in a  
1185 row is given on the right.

1186

1187 **Figure 1-figure supplement 2. Separation of heads and flagella from whole sperm**

1188 Dark-field micrographs of whole sperm (left), purified heads (middle), and purified flagella  
1189 (right). Bar represents 100  $\mu\text{m}$ .

1190

1191 **Figure 1-figure supplement 3. Electrophysiological characterization of currents**  
1192 **recorded from zebrafish sperm**

1193 (A) Whole-cell recordings at different intracellular  $\text{Cl}^-$  concentrations ( $\text{Cl}_i$ ).

1194 (B) IV relations from part A.

1195 (C) Reversal potentials ( $V_{\text{rev}}$ ) from whole-cell recordings at different extracellular  $\text{K}^+$  ( $\text{K}_o$ ) and  
1196 intracellular  $\text{Cl}^-$  concentrations ( $\text{Cl}_i$ ) in whole sperm and isolated heads. Individual data  
1197 (symbols) and mean  $\pm$  sd (gray bars), number of experiments in parentheses.

1198

1199 **Figure 2-source data 1. Indicators of merit for the mass spectrometric results of testis**  
1200 **preparation**

1201 <sup>a</sup> m, indicates oxidized methionine, <sup>b</sup>  $\Delta M$  [ppm] relative mass error, <sup>c</sup> XCorr,  $\Delta Score$  and  $\Delta Cn$   
1202 indicate results based on searches with the sequest algorithm in Proteome Discoverer; <sup>d</sup> PEP  
1203 (Posterior Error Probability) describes the probability that the observed hit is a chance event.

1204

1205 **Figure 2-source data 2. Indicators of merit for the mass spectrometric results of**  
1206 **different sperm preparations: whole sperm, head and flagella**

1207 <sup>a</sup> m, indicates oxidized methionine, <sup>b</sup>  $\Delta M$  [ppm] for all peptides is below  $\pm 2.5$ , <sup>c</sup> XCorr,  
1208 indicates results based on searches with the sequest algorithm; Amanda, indicates results  
1209 based on searches with the MS Amanda algorithm, <sup>d</sup> PEP (Posterior Error Probability)  
1210 describes the probability that the observed hit is a chance event;  $\Delta Score$  and  $\Delta Cn$  are not  
1211 indicated separately since the scores for all peptides are 1 and 0, respectively.

1212

1213 **Figure 3-figure supplement 1.  $K^+$  dependence of heterologously expressed *DrCNGK***  
1214 **channels in oocytes and channel block by tetraethylammonium (TEA)**

1215 (A) Two-Electrode Voltage-Clamp recordings of heterologously expressed *DrCNGK*  
1216 channels in the presence of different  $K^+$  concentrations (left panel: 7 mM, middle panel:  
1217 96 mM) and corresponding IV relation (right panel).

1218 (B) Two-Electrode Voltage-Clamp recordings of uninjected oocytes (control) in the presence  
1219 of different  $K^+$  concentrations (left panel: 7 mM, middle panel: 96 mM). (C) Pooled IV curves  
1220 of Two-Electrode Voltage-Clamp recordings of *DrCNGK*-injected and uninjected oocytes

1221 (control) in the presence of different  $K^+$  concentrations (left panel: 7 mM, middle panel:  
1222 96 mM). Number of experiments is given in parentheses.

1223 (D) Reversal potentials ( $V_{rev}$ ) of *DrCNGK*-injected and control oocytes in the presence of  
1224 different  $K^+$  concentrations. Number of experiments is given in parentheses.

1225 (E) Whole-cell recordings from zebrafish sperm and Two-Electrode Voltage-Clamp  
1226 recordings from heterologously expressed *DrCNGK* channels in the absence and presence of  
1227 different TEA concentrations (0, 1, and 100 mM TEA).

1228 (F) Normalized ( $I-I_{minFit}/I_{maxFit}$ ) dose dependence of TEA block. Mean current  $\pm$  sd. Individual  
1229 dose response curves were fitted with the Hill equation. Mean ( $\pm$  sd)  $K_i$  value and Hill  
1230 coefficient for sperm  $K^+$  current were  $4.5 \pm 1.1$  mM and  $1.0 \pm 0.2$  ( $n = 5$ ) and for *DrCNGK* in  
1231 oocytes  $1.6 \pm 0.3$  mM and  $1.0 \pm 0.1$  ( $n = 11$ ), respectively. The solid lines were calculated  
1232 with the Hill equation using mean values for  $K_i$  and the Hill coefficient.

1233

1234 **Figure 3-figure supplement 2. Sequence alignment of the individual CNBDs from the**  
1235 ***DrCNGK* and *ApCNGK* channels**

1236 The secondary structure elements of CNBDs are indicated above the sequences. A key Arg  
1237 residue between  $\beta 6$  and  $\beta 7$  is indicated by an asterisk. An FGE motif important for interaction  
1238 with cyclic nucleotides and highly conserved Gly residues that are important for the CNBD  
1239 fold are highlighted in yellow.

1240

1241 **Figure 3-figure supplement 3. Photo-release of cyclic nucleotides in HEK cells**  
1242 **expressing *ApCNGK* channels and use of 8Br-analogs in *ApCNGK*-injected oocytes.**

1243 (A) Left and middle panel: Pooled IV curves of *Ap*CNGK channels heterologously expressed  
1244 in HEK cells before (-cGMP or -cAMP) and after the release of cGMP or cAMP. Cells were  
1245 loaded with 100  $\mu$ M BCMACM-GMP or BCMACM-cAMP. Right panel: Whole-cell  
1246 recordings at +15 mV from HEK cells heterologously expressing *Ap*CNGK channels loaded  
1247 with 100  $\mu$ M BCMACM-caged cGMP (upper panel) or BCMACM-caged cAMP (lower  
1248 panel). Arrows indicate the delivery of the UV flash to release cyclic nucleotides by  
1249 photolysis. (B) Pooled IV curves of Two-Electrode Voltage-Clamp recordings of *Ap*CNGK-  
1250 injected oocytes in the presence and absence of 3 mM 8Br-cGMP.

1251

1252 **Figure 3-figure supplement 4. Photo-release of cyclic nucleotides (A) or  $\text{Ca}^{2+}$  (B) in**  
1253 **sperm.**

1254 (A) Mean velocity (averaged-path velocity, VAP) before (-) and after (+) release of cAMP or  
1255 cGMP. Sperm were loaded with 30  $\mu$ M DEACM-caged cAMP or DEACM-caged cGMP.  
1256 Individual data (symbols) and mean  $\pm$  sd (gray bars), number of experiments in parentheses.  
1257 (B) Mean velocity (VAP) before and after the 1<sup>st</sup> (+) and 2<sup>nd</sup> (++) UV flash. Statistics as in  
1258 part A.

1259

1260 **Figure 3-figure supplement 5. Control of loading and release of DEACM-cAMP in**  
1261 **zebrafish sperm.**

1262 (A) Dark-field micrograph of sperm loaded with DEACM-caged cAMP (30  $\mu$ M) using red  
1263 light. (B) Fluorescence image after 15 s of continuous illumination with 365 nm UV light  
1264 (1.75 mW power). (C) Time course of the release for the cell marked with a red circle.

1265

1266 **Figure 5-figure supplement 1. pH dependence of heterologously expressed *DrCNGK***  
1267 **channels in oocytes.**

1268 Two-Electrode Voltage-Clamp recordings of *DrCNGK*-injected (A) and uninjected (B)  
1269 oocytes. Cells were reversibly perfused with 96 mM K<sup>+</sup> bicarbonate followed by 1 mM  
1270 NH<sub>4</sub>Cl added to K<sup>+</sup> gluconate (10 min each). Voltage steps from -100 mV to + 30 mV from a  
1271 holding potential of -60 mV.

1272

1273 **Figure 5-figure supplement 2. High intracellular Ca<sup>2+</sup> does not suppress *DrCNGK***  
1274 **currents.**

1275 Pooled IV relations of whole-cell recordings from whole sperm and isolated heads under  
1276 standard conditions (ES/IS, pH 7.4) (Figure 1G) and from whole sperm; the [Ca<sup>2+</sup>]<sub>i</sub> in the  
1277 pipette solution was adjusted to 1 μM.

1278

1279 **Figure 5-figure supplement 3. Hypoosmotic conditions do not stimulate or diminish**  
1280 ***DrCNGK* currents in *Xenopus* oocytes.**

1281 *DrCNGK*-injected oocytes were recorded in the TEVC mode in ND96-7K and ND48-7K  
1282 solutions (n = 4). No significant differences were observed.

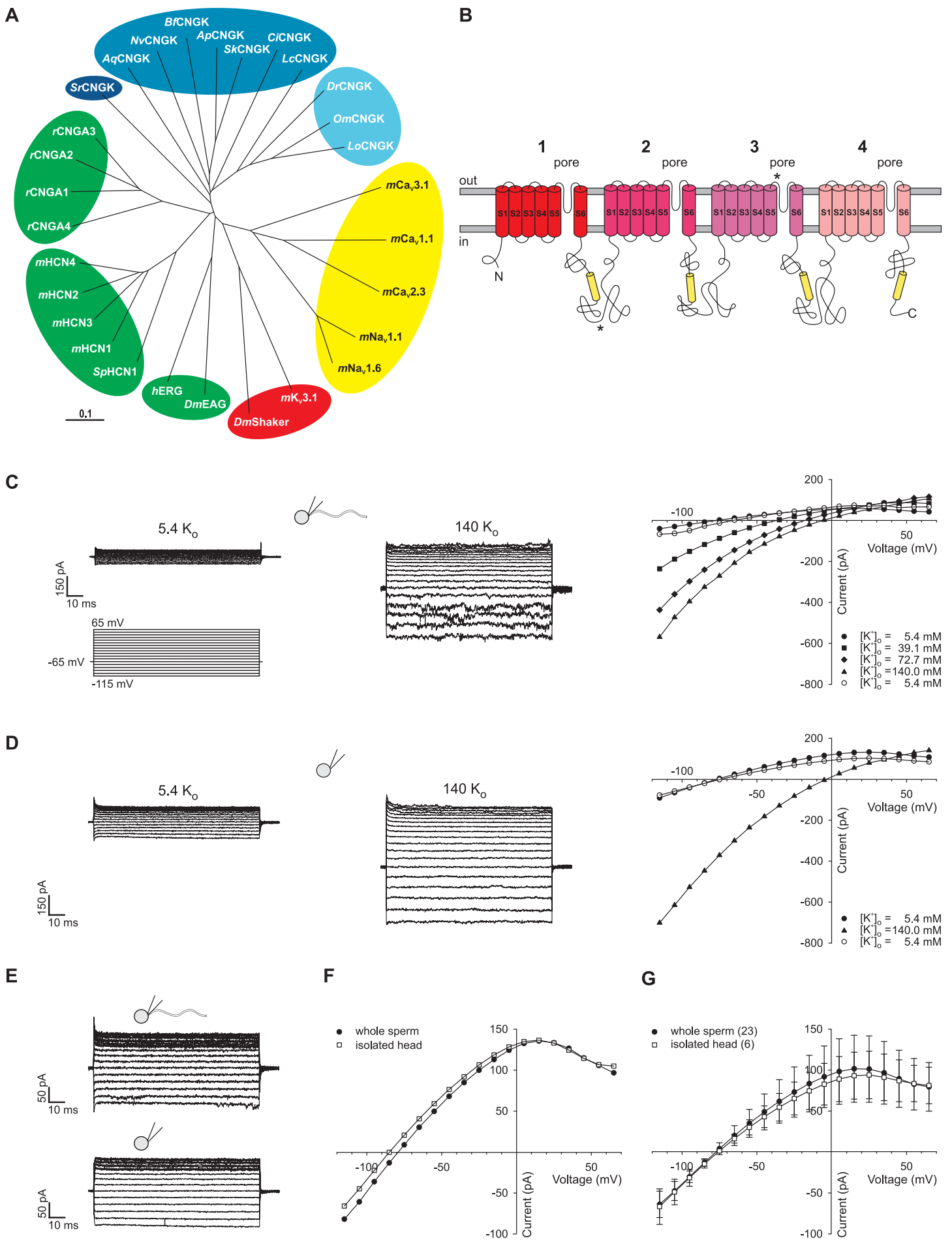


Figure 1 Fechner et al.

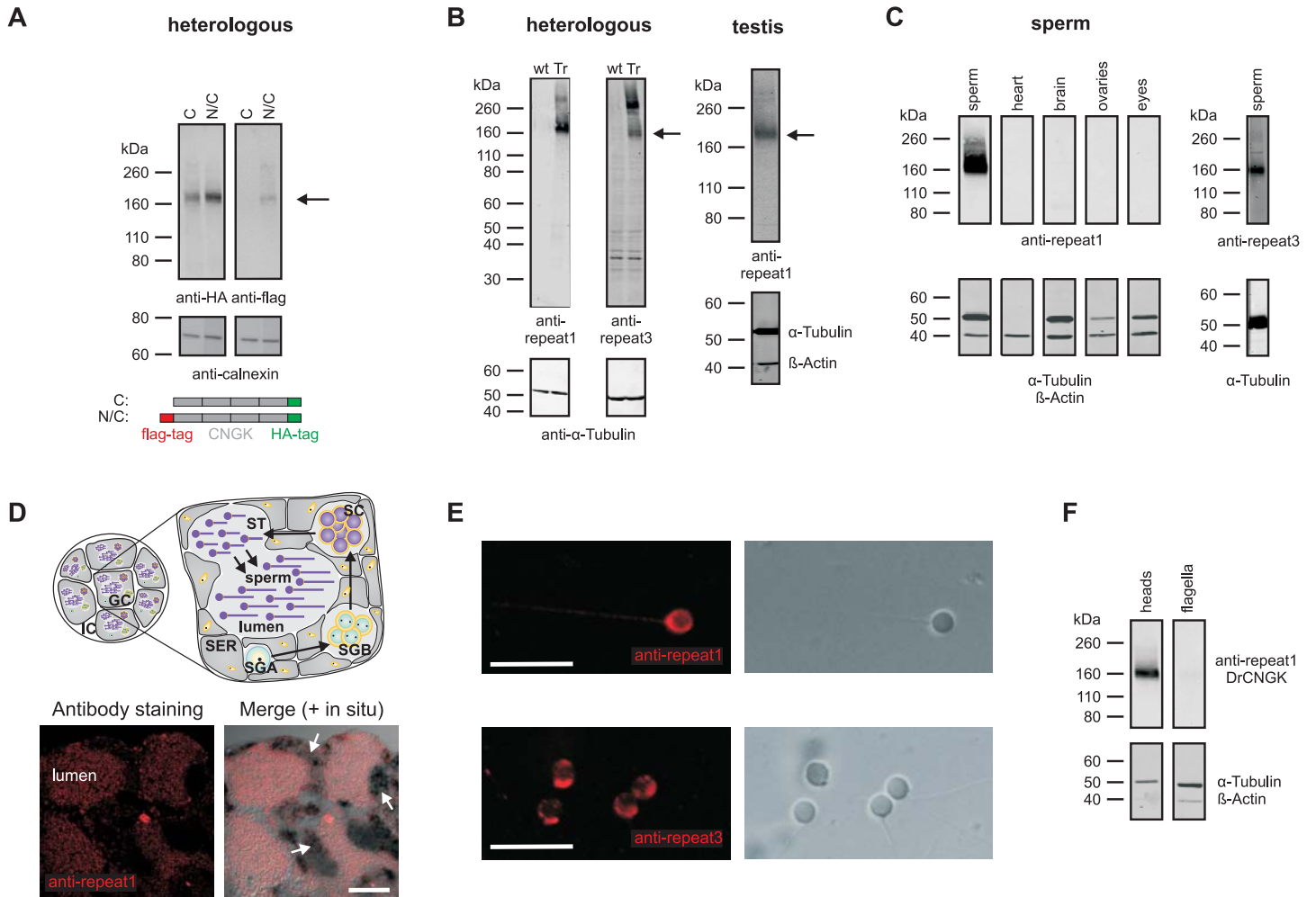


Figure 2 Fechner et al.

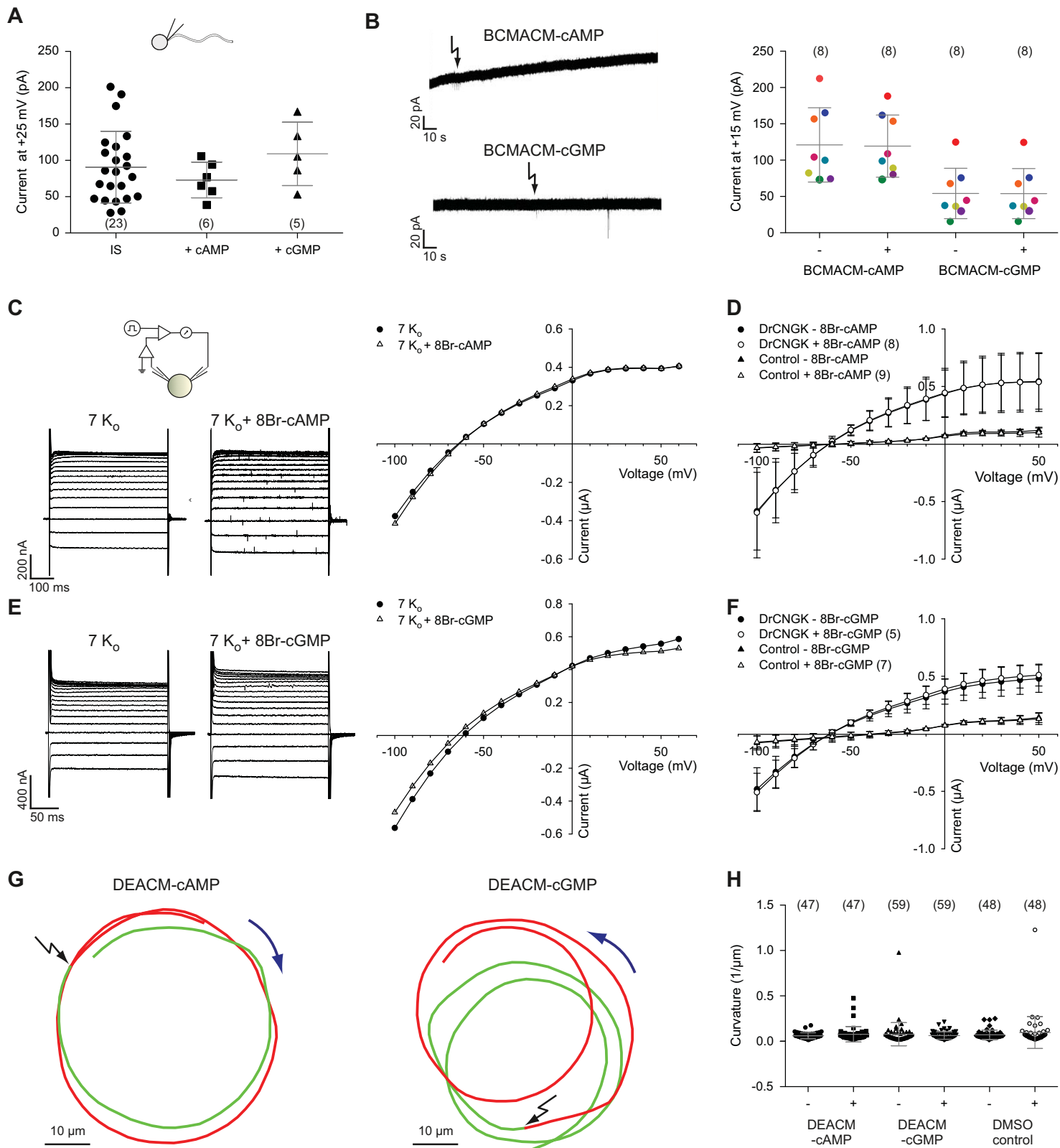


Figure 3 Fechner et al.

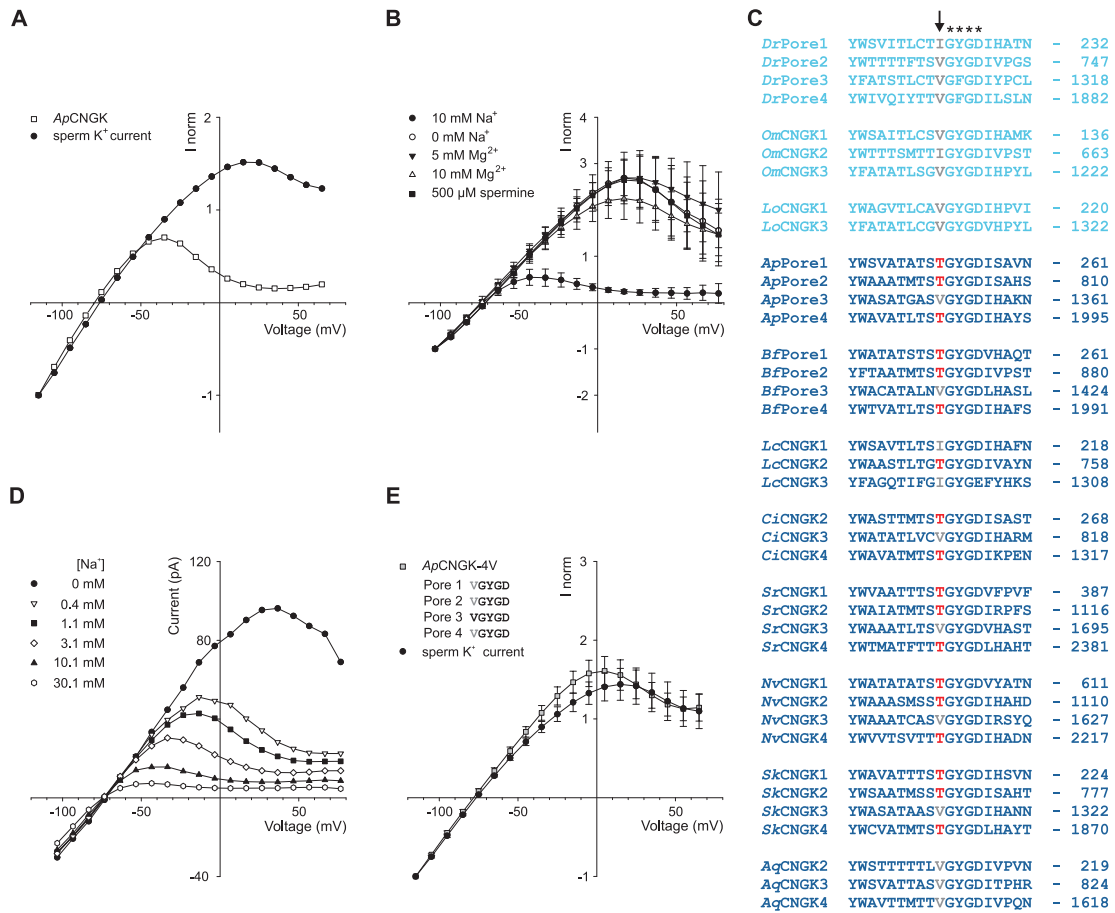


Figure 4 Fechner et al.

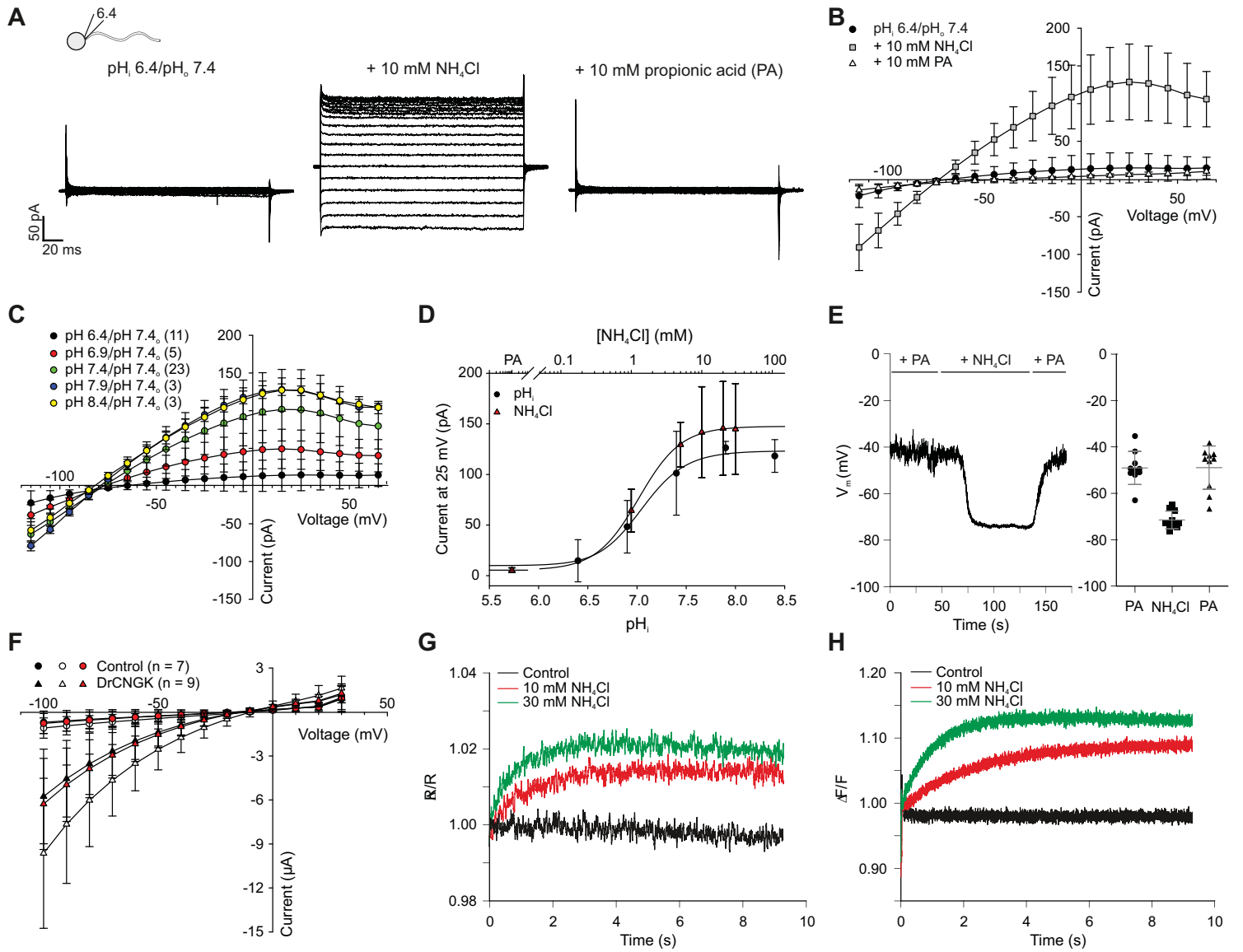


Figure 5 Fechner et al.

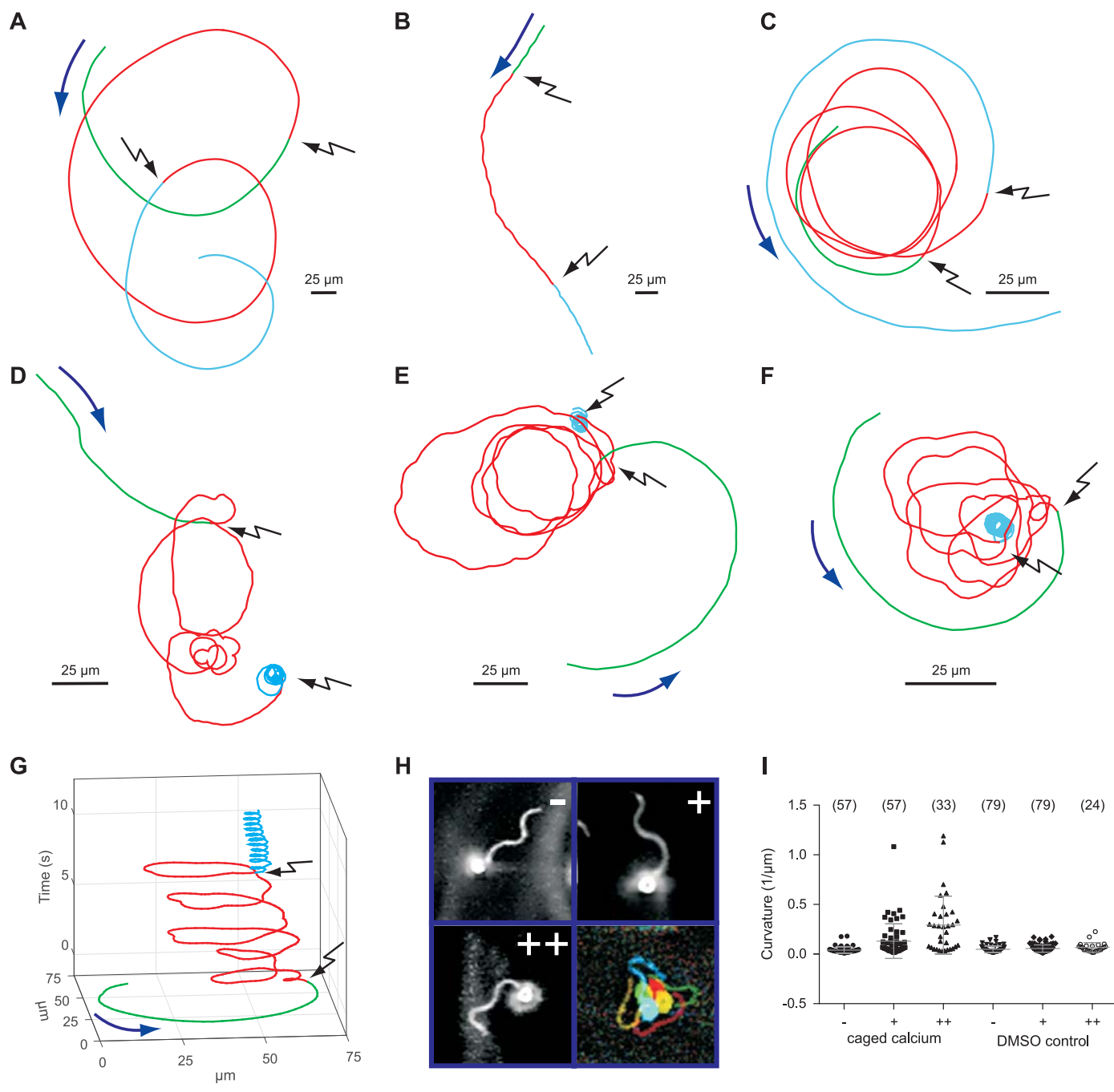


Figure 6 Fechner et al.

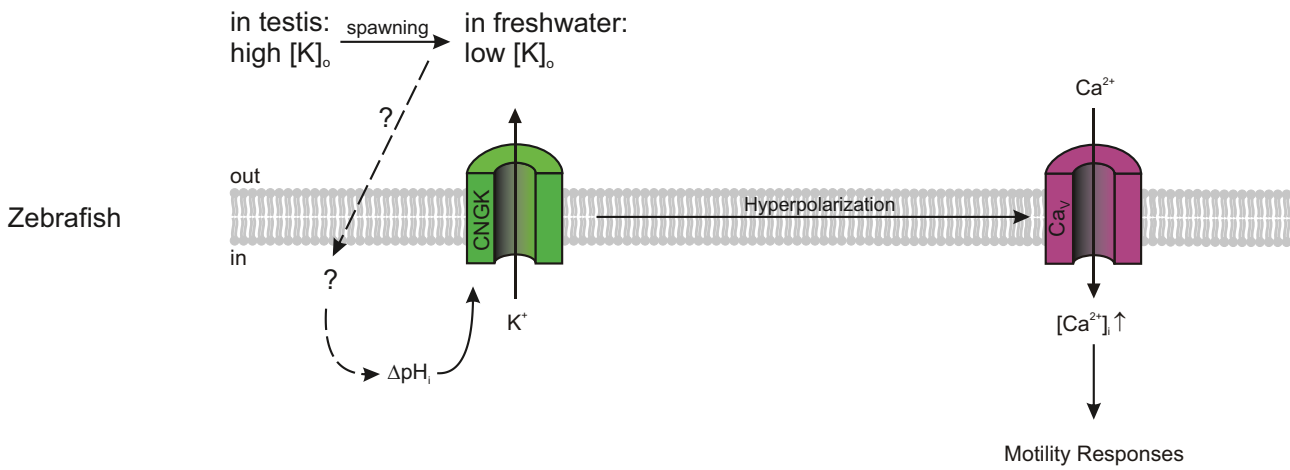
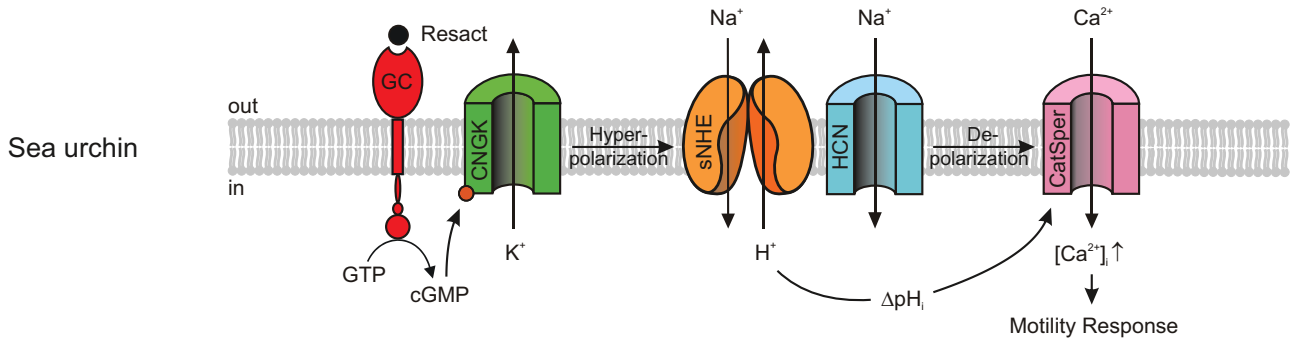


Figure 7 Fechner et al.